Toxicology in Vitro 81 (2022) 105333

Contents lists available at ScienceDirect

Toxicology in Vitro

journal homepage: www.elsevier.com/locate/toxinvit

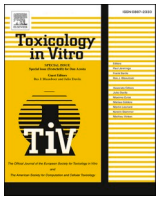

An *in vitro* strategy using multiple human induced pluripotent stem cell-derived models to assess the toxicity of chemicals: A case study on paraquat

Carolina Nunes [a,b,1], Pranika Singh [c,d,1], Zahra Mazidi [e,f,1], Cormac Murphy [g,1], Aurore Bourguignon [h,i], Sara Wellens [j], Vidya Chandrasekaran [g], Sreya Ghosh [k], Melinda Zana [h], David Pamies [a,b], Aurélien Thomas [l,m], Catherine Verfaillie [k], Maxime Culot [j], Andras Dinnyes [h,i,n], Barry Hardy [c], Anja Wilmes [g], Paul Jennings [g], Regina Grillari [e], Johannes Grillari [e,f,o], Marie-Gabrielle Zurich [a,b,*,2], Thomas Exner [c,p,*,2]

[a] *Department of Biomedical Sciences, University of Lausanne, Rue du Bugnon 7, 1005 Lausanne, Switzerland*
[b] *Swiss Centre for Applied Human Toxicology (SCAHT), University of Basel, Missionsstrasse 64, 4055 Basel, Switzerland*
[c] *Edelweiss Connect GmbH, Technology Park Basel, Hochbergerstrasse 60C, 4057 Basel, Switzerland*
[d] *Division of Molecular and Systems Toxicology, Department of Pharmaceutical Sciences, University of Basel, Klingelbergstrasse 50, 4056 Basel, Switzerland*
[e] *Evercyte GmbH, Vienna, Austria*
[f] *Institute of Molecular Biotechnology, Department of Biotechnology, BOKU - University of Natural Resource and Life science (BOKU), Vienna, Austria*
[g] *Division of Molecular and Computational Toxicology, Department of Chemistry and Pharmaceutical Sciences, AIMMS, Vrije Universiteit Amsterdam, De Boelelaan 1108, 1081 HZ Amsterdam, the Netherlands*
[h] *BioTalentum Ltd, Gödöllő, Hungary*
[i] *Department of Physiology and Animal Health, Institute of Physiology and Animal Health, Hungarian University of Agriculture and Life Sciences, Gödöllő, Hungary*
[j] *University of Artois, UR 2465, Laboratoire de la Barrière Hémato-Encéphalique (LBHE), Faculté des sciences Jean Perrin, Rue Jean Souvraz SP18, F-62300 Lens, France*
[k] *Department of Development and Regeneration, Stem Cell Institute, KU Leuven, Leuven, Belgium*
[l] *Unit of Forensic Toxicology and Chemistry, CURML, Lausanne and Geneva University Hospitals, Geneva, Switzerland*
[m] *Faculty Unit of Toxicology, CURML, Faculty of Biology and Medicine, University of Lausanne, Lausanne, Switzerland*
[n] *Department of Cell Biology and Molecular Medicine, University of Szeged, Szeged, Hungary*
[o] *Ludwig Boltzmann Institute for Traumatology Research Center in cooperation with AUVA, Vienna, Austria*
[p] *Seven Past Nine d.o.o., Hribljane 10, 1380 Cerknica, Slovenia*

ARTICLE INFO

Editor: Dr. P. Jennings

Keywords:
Human induced pluripotent stem cells
Paraquat
New approach methodology
Toxicology
Acute toxicity

ABSTRACT

Most OECD guidelines for chemical risk assessment include tests performed on animals, raising financial, ethical and scientific concerns. Thus, the development of human-based models for toxicity testing is highly encouraged. Here, we propose an *in vitro* multi-organ strategy to assess the toxicity of chemicals. Human induced pluripotent stem cells (hiPSCs)-derived models of the brain, blood-brain barrier, kidney, liver and vasculature were generated and exposed to paraquat (PQ), a widely employed herbicide with known toxic effects in kidneys and brain. The models showed differential cytotoxic sensitivity to PQ after acute exposure. TempO-Seq analysis with a set of 3565 probes revealed the deregulation of oxidative stress, unfolded protein response and estrogen receptor-mediated signaling pathways, in line with the existing knowledge on PQ mechanisms of action. The main advantages of this strategy are to assess chemical toxicity on multiple tissues/organs in parallel, exclusively in human cells, eliminating the interspecies bias, allowing a better evaluation of the differential sensitivity of the

Abbreviations: 3Rs, Replacement, Reduction and Refinement of Animal Experiments; BBB, Blood-brain barrier; BLECs, Brain-like endothelial cells; BS, BrainSphere; DEG, Differentially expressed gene; EC, Endothelial cell; ER, Endoplasmic Reticulum; ESC, Embryonic stem cell; ESCs, Embryonic stem cells; ESR, Estrogen Receptor; hiPSC, Human induced pluripotent stem cell; HLC, Hepatocyte-like cell; LFC, log2 fold change; NAM, New approach methodology; NC, Neural cell; PODO, Podocyte; PTL, Proximal Tubular like cell; ROS, Reactive oxygen species; UPR, Unfolded protein response.

* Corresponding authors.
E-mail addresses: mzurich@unil.ch (M.-G. Zurich), thomas.exner@sevenpastnine.com (T. Exner).
[1] Shared first authorship.
[2] Shared senior authorship.

https://doi.org/10.1016/j.tiv.2022.105333
Received 27 August 2021; Received in revised form 4 December 2021; Accepted 11 February 2022
Available online 16 February 2022

models representing the diverse organs, and increasing the chance to identify toxic compounds. Furthermore, although we focused on the mechanisms of action of PQ shared by the different models, this strategy would also allow for organ-specific toxicity testing, by including more cell type-specific probes for TempO-Seq analyses. In conclusion, we believe this strategy will participate in the further improvement of chemical risk assessment for human health.

1. Introduction

The need to develop new approach methodologies (NAMs) providing mechanistic understanding for toxicology testing is now well recognized, and governmental agencies worldwide have been pushing towards the development of human-based assays for human safety assessment (EUR-Lex, 2010; National Research Council, 2007; Oredsson et al., 2019; Sewell et al., 2017). For instance, the US Environmental Protection Agency plans to eliminate animal testing from regulatory requirements for pesticides and industrial chemicals by 2035 (EPA, 2019). However, the move from animal experimentation to NAMs highly depends on the ability of the NAMs to mirror human rather than animal physiology (Herrmann et al., 2019). Since their development, a little over a decade ago (Takahashi et al., 2007), human induced pluripotent stem cells (hiPSCs) have represented a potential paradigm shift across the biological sciences from developmental biology to regenerative medicine. For the field of toxicology, they have been seen as a valuable new tool to enable NAMs to achieve the ideals of the 3Rs through the production of *in vitro* models with human relevant phenotypes that can replace animal testing (Steimberg et al., 2020). While they share capacity for self-renewal and pluripotent potential of embryonic stem cells (ESCs), their generation from adult somatic cells come with a range of advantages while avoiding some of the controversies associated to ESCs (Liu et al., 2017). The relative ease by which hiPSCs can be generated from cells obtained with minimal discomfort on the part of the donor, from sources such as blood, skin and even urine (Zhou et al., 2011), has allowed for the establishment of large cell banks. StemBANCC is one such bank that generated hiPSCs lines from 500 healthy and diseased individuals, and most of these well described lines are now widely available for drug and chemical screening (Morrison et al., 2015) through the European Bank For Induced Pluripotent Stem Cells (EBiSC).

While traditionally, cancer or immortalised cell lines, and to a lesser extent, primary cells, have been the main cell sources for *in vitro* chemical safety assessment, each have their own drawbacks that hiPSCs can potentially overcome. Human primary cells, that would be the most adequate cells to use, can be difficult to obtain and are only available in a limited quantity for a limited time, while undifferentiated hiPSCs can, in theory, proliferate indefinitely. Immortalised cell lines, once made, can be continuously available; however, these models often lack some important biological aspects of their unaltered counterparts leading to concerns that they may be poor models for healthy human cells and lack the sensitivity for toxicity testing (Liu et al., 2017). While hiPSCs have their own challenges, chief among them being the establishment of robust and repeatable differentiation protocols that produce the desired cell type, once this is done, they are a renewable source of cells that can express many important intrinsic phenotypic features often lost in traditional cell lines. For example, a recently published hiPSC differentiation protocol produces kidney proximal tubular-like cells that, alongside other characteristic markers, expressed megalin (LRP2), an apical transporter that plays a key role in reabsorption and is absent in most available human immortalised cell lines (Chandrasekaran et al., 2021).

With the establishment of reliable differentiation protocols for more cell types, and with the emergence of complex culture systems, the possibility has emerged to use hiPSC-derived cells to model the impact of toxins on the different cell types/organs from the same human donor. In this study, we hypothesized that an *in vitro* multi-organ human iPSC-derived strategy will allow the reliable assessment of the toxicity of chemicals. To test this, hiPSCs-derived models of the brain (2D and 3D mixed-cell cultures), blood-brain barrier (brain capillary endothelial cells), kidney (podocytes and proximal tubular cells), liver (hepatocyte) and vasculature (endothelial cells) were generated from two donors, using published or newly developed protocols, and were exposed to paraquat (PQ), a widely employed herbicide used as a reference compound chosen for its known toxic effects on a range of tissues across the body (Cicchetti et al., 2009; Dinis-Oliveira et al., 2008; Gao et al., 2020). TempO-Seq analysis showed the disruption of "Oxidative stress induced gene expression via Nrf2 markers", as expected since oxidative stress is the well-known PQ mechanism of action, but also of two other pathways previously demonstrated to be involved in PQ toxicity, "Unfolded protein response" and "ESR-mediated signaling", suggesting this strategy as a future tool for prioritization, screening of chemicals and risk assessment.

2. Materials and method

2.1. Cell cultures

Human iPSCs used in this study (SBAD3 clone 1 and SBAD2 clone 1) were generated in the IMI-funded StemBANCC project (http://stembancc.org) (Morrison et al., 2015) from purchased primary fibroblasts of non-diseased donors (Lonza). They were cultured on Matrigel® Growth Factor Reduced (GFR) (Corning) or Geltrex® (Gibco) in mTeSR™1 (StemCell Technology) feeder-free medium at 37 °C in a humidified 5% CO_2 incubator. Medium was replaced every day and cells were passaged every 4–5 days using Versene® according to the supplier's protocol (Thermo Fisher Scientific).

Human iPSCs were differentiated into different cell types to obtain *in vitro* models for several tissues/organs. Details on methodologies and characterization are found in the references given for each model, in Chandrasekaran et al. (in preparation – for this special issue), as well as in Table 1. BrainSpheres (BS), a 3D model containing neurons, astrocytes and oligodendrocytes, were prepared from neuroprogenitor cells (NPCs) derived from the SBAD3 clone 1 using a Gibco protocol (Nunes and Zurich, 2020; Pamies et al., 2017). Neural cells (NC), a 2D model containing neurons and astrocytes were generated from NPCs derived from the SBAD2 clone 1 using dual SMAD inhibition protocol (Chambers et al., 2009; Chandrasekaran et al., 2017; Lo Giudice et al., 2019; Ochalek et al., 2017). The brain-like endothelial cells (BLECs) transwell model was prepared from the SBAD3 clone 1 (Sevin et al., 2019; Wellens et al., 2021). The kidney cells, podocytes (PODO) (Murphy et al., 2019; Rauch et al., 2018) and proximal tubular like cells (PTL) (Chandrasekaran et al., 2021) were derived from the SBAD2 clone 1 containing a Green Fluorescent Protein (GFP) tag downstream of one allele of the HMOX-1 gene (SBAD2 clone 1 HMOX1-eGFP, prepared by Prof. Dinnyes's laboratory, Biotalentum, Hungary), although this fluorescent property was not utilised in this study. The endothelial cells (EC) (Gholami et al., 2021) representing the vascular system and the hepatocyte-like cells (HLC) (Boon et al., 2020) representing the liver were derived from SBAD2 clone 1.

2.2. Paraquat exposure

PQ (Sigma–Aldrich, catalogue No 36541, lot #BCBW5264, CAS #75365-73-0) was dissolved in ultrapure water. The different cell cultures were exposed to PQ for 24 h and BS was also exposed for 48 h, after

Table 1
Characterization overview of the different models used.

Name	Organ	References	Time in culture before exposure	Characterization							Functional Assay	
				Cell Type	Marker	Technique (Ref at protocol DOI)					Assay	Observations
						RT-qPCR	Immunocytochemistry	FACS	Western-blot	TempO-Seq		
BS	Brain	[1]. Pamies et al., 2017	42d	Neurons	ACHE					x	Multi-Electrode Array MEA (Pamies et al., 2017)	Electrical activity
					B3T					x		
					GABRA1	x [1]				x		
					GAD1	x [1]				x		
					GRIN1	x [1]				x		
					MAP2		x [1]			x		
					NFH		x [1]			x		
					SYN	x [1]	x [1]			x		
					SYP					ND		
					TH	x [1]	x [1]			x		
					TUJ1		x [1]			NP		
					VGLUT1		x [1]			x		
				Astrocytes	GFAP	x [1]	x [1]			x		
					S100	x [1]				ND		
					VIM					x		
				Oligodendrocytes	CNPase		x [1]			NP		
					MBP	x [1]	x [1]			x		
					NOGOA		x [1]			NP		
					O1	–	x [1]			NP		
					O2	–	x [1]			NP		
					O4	–				NP		
					OLIG2	x[1]				x		
NC	Brain	[1]. Ochalek et al., 2017, [2]. Chandrasekaran et al., 2017	21d	Neurons	TUBB3	x[2]	x [1, 2]			x	Calcium current measurements (Lo Giudice et al., 2019) and patch clamp (Chandrasekaran et al., 2017)	Electrical activity at later time-points
					MAP2	x[2]	x [1, 2]			x		
					NF200		x [1]			NP		
				NPC	Ki67	x[2]	x[2]			NP		
					SOX1	x[2]	x[2]	x[2]		x		
					NESTIN	x[2]	x [1, 2]	x [1, 2]		NP		
					PAX6	x[2]	x [1, 2]	x [1, 2]		NP		
					SOX9	x[2]		x[2]		NP		
				Astrocytes	GFAP	x[2]	x[2]			x		
					AQP4	x[2]	x[2]			NP		
BLECs	BBB	[1]. Wellens et al., 2021	8d	Brain-like endothelial cells	ABCG2					x 1	Pump-out assay (Wellens et al., 2021 and Sevin et al., 2019)	Reduced Rhodamine123 extrusion under influence from elacridar and verapamil efflux pump inhibitors.
					ABCB1					x [1]		
					CDH5		x [1]			x [1]		
					CLDN5		x [1]			ND		
					vWF					x [1]		
					CD31		ND			ND		
					ABCC4					x [1]		
					ABCC5					x [1]		
					SLC25A46					x [1]		
					SLC26A2					x [1]		
					SLC27A2					x [1]		
					SLC27A3					x [1]		
					SLC2A1					x [1]		
					SLC35A3					x [1]		
					SLC7A5					x [1]		
EC	Vasculature	[1]. Gholami et al., 2021	8d	Endothelial cells	TBXT	x [1]				NP	Matrigel assay	Endothelial cells could form tubes at one of the beginning stages of angiogenesis
					CD31	x [1]	x [1]	X [1]		x		
					CDH5	x [1]	x [1]	x [1]		NP		

(*continued on next page*)

Table 1 (*continued*)

Name	Organ	References	Time in culture before exposure	Characterization			Technique (Ref at protocol DOI)					Functional Assay	
				Cell Type	Marker		RT-qPCR	Immunocytochemistry	FACS	Western-blot	TempO-Seq	Assay	Observations
					VEGFR2				x [1]		NP		
					vWF			x [1]			ND		
PTL	Kidney	[1]. Chandrasekaran et al., 2021	14d	Proximal tubule-like cells	LRP2			x [1]		x [1]	NP	Parathyroid hormone (PTH) response assay; Calcein-AM efflux assay; Albumin uptake assay for megalin facilitated endocytosis	Increase levels of cAMP in response to PTH; Functional P-gp efflux; uptake of labelled albumin
					TJP3			x [1]			NP		
					PTH1R						NP		
					FBP1						NP		
PODO	Kidney	[1]. Rauch et al., 2018, [2]. Murphy et al., 2019	12-14d	Podocytes	WT1			x [1,2]		x [1]	ND	Albumin uptake assay	Uptake of albumin by podocyte-like cells
					SYNPO		x [1]	x [1,2]		x [1]	NP		
					NPHS1			x [1]		x [1]	NP		
					NPHS2			x [1]		x [1]	NP		
HLC	Liver	[1]. Ghosh et al. (under revision for this special issue)	42d	Hepatocyte-like cells	ALB		x [1]				x	Albumin secretion assay; CYP3A4 activity assay	Albumin secretion was observed at about 40% of that of primary hepatocytes plated for 12 h. CYP3A4 activity was observed (about one-third that of primary hepatocytes).
					AFP		x [1]	x [1]			x		
					HNF4A		x [1]	x [1]			x		
					CYP3A4		x [1]	x [1]			x		
					CYP2C9		x [1]				x		
					G6PC		x [1]				x		
					PEPCK		x [1]				NP		
					SLC10A1		x [1]				x		
					SERPINA1						x		

NT: Non tested; x: detected; ND: not detected; NP: not present in the TempO-Seq panel; Superscript number: refers to publication listed under references column.

various duration in culture, corresponding to a maturation state defined by each lab. BS was exposed to PQ at day *in vitro* (DIV)42, NC at DIV21, BLECs at DIV8, PODO at DIV12-14, PTL at DIV14, EC at DIV8, and HLC at DIV40. Concentrations of paraquat are given in figure or figure captions (Figs. 2, 3 and Table 2). For cytotoxicity testing, 2–9 samples were run per group, and for TempO-Seq analysis 2–16 samples were run per group. Exposure of the cell models to PQ was conducted in 6 different labs, NC at BioTalentum Ltd. (Hungary), BS at University of Lausanne (Switzerland), PODO and PTL at Vrije Universiteit Amsterdam (Netherlands), EC at Evercyte GmbH (Austria), HLC at Katholieke Universiteit Leuven (Belgium) and BLECs at Université d'Artois (France).

2.3. Cytotoxicity assays

After exposure of the different iPSC-derived cell models to a large range of PQ concentrations, viability assays were run in order to establish cytotoxicity concentration-dependent curves.

2.3.1. Resazurin assay

After treatment with PQ, the medium was removed and the cells were incubated with 44 μM resazurin diluted in cell culture medium for a duration indicated in Table 2. The fluorescent product resorufin was measured at 530–560 nm excitation and 590 nm emission using a plate reader. After subtraction of the background (only resazurin solution), results of the treated cultures were expressed as percentage of the mean of the control cultures.

2.3.2. ATP assay

ATP viability assay was performed using the CellTiter-Glo® 3D Cell Viability Assay, according to the manufacturer's protocol (Promega). NC were lysed with 100 μL CellTiter-Glo® 3D Reagent for 90 min at RT. Luminescence signal was recorded with a Thermo VarioScan Flash plate reader (Thermo Fisher Scientific). Results of the treated cultures were expressed as percentage of the mean of the control cultures.

2.4. TempO-Seq sample collection

Samples of the different cell systems were treated with PQ at concentrations chosen on the basis of the previously established cytotoxicity curves (final concentrations and time points in Table 2 and indicated in figure captions). DMSO was added to all samples (final concentration 0.01%) due to the simultaneous testing of water-insoluble chemicals (results not presented in this manuscript). At the end of exposure, cells were collected and lysed with 1× TempO-Seq Lysis Buffer in a ratio of 0.25 to 2 million cells/mL. Lysates were frozen at −80 °C and shipped to BioClavis Technologies Ltd. (Glasgow) on dry ice where the TempO-Seq assay using the EU-ToxRisk v2.1 panel (3565 probes representing 3257 genes) was conducted with standard attenuators. The service also included primary processing to derive gene-annotated raw read counts and quality control, following a previously described procedure (Limonciel et al., 2018; Mav et al., 2018). Each sample FASTQ file was aligned against the TempO-Seq transcriptome using the Bowtie aligner (Li and Durbin, 2009). The output of this analysis generated a table of counts per gene per sample.

2.5. TempO-Seq data analysis and visualization

2.5.1. Sample and probe filtering

The raw read count data of the samples provided by BioClavis was used for differential expression analysis. The raw data and corresponding metadata files were uploaded and maintained on an internal instance of the EdelweissData™ management system (SafeRworldbyDesign2020) for easier accessibility. All samples exposed to PQ and the respective controls from the different hiPSC-derived cell models were extracted using a python workflow as previously described (Singh et al., 2021).

Table 2
Description of all models used in the study and respective IC50/30/20/10 and PQ concentrations used for TempOSeq. BrainSpheres (BS), Neural Cells (NC), Blood-Brain Barrier (BBB), Endothelial cells (EC), renal proximal tubular epithelial-like cells (PTL) podocytes (PODO), hepatocytes-like cells (HLC).

Model	Organ	PQ exposure (h)	Cytotoxicity						TempOSeq
			Assay for assessment	Incubation time (h)	Concentration (μM)				Concentrations (μM)
					IC50	IC30	IC20	IC10	
BS	Brain	24	Resazurin	3	200	161	132	97	-
		48			60	51	45	38	1–2.5–5
NC	Brain	24	ATP	1 h30	49	31	24	16	0.05–0.1
BLECs	BBB	24	Resazurin	2-2 h30	749	654	132	97	50–100–250
EC	Vasculature	24	Resazurin	1 h30	114	55	35	17	1.25–2.5–5
PTL	Kidney	24	Resazurin	1	561	405	327	237	25–100–300
PODO	Kidney	24	Resazurin	2	373	164	97	45	5–50–100
HLC	Liver	24	Resazurin	2	–	–	–	–	12.5–25–50–100
		48			1093	797	590	376	-

Before downstream analyses (Fig. 1), samples and probes were quality controlled. The samples were checked as described elsewhere (Singh et al., 2021) by investigating a) the total number of probe read counts per sample with a threshold of 50,0000 under which samples were removed and b) the Pearson's correlation coefficient among replicates using Morpheus online tool with a threshold of 0.80 under which samples were removed. Concerning the probes, only the ones with median of raw read counts higher than 5 across all conditions for each model were used.

2.5.2. Differential expression analysis

The filtered raw data was analysed for differential expression using the R based library DESeq2 (Love et al., 2014). Samples underwent an r-log transformation and posterior unsupervised clustering using standard DeSeq2 suggested settings to visualize the variance within and between different cell models, as well as between treatment and control groups. Differential expression analysis was performed using DeSeq2 library after normalization of read counts using its standard mean-median ratio method. An automatic script (Singh et al., 2021) was used to generate the statistical values log2fold changes, adjusted *p*-values and base means. To select the most significantly expressed probes in each cell model for further analyses, thresholds were set at: log2 fold changes $> |0.58|$ and adjusted *p*-values <0.05.

2.5.3. Gene-pathway association

ConsensusPathDB (v.34) (http://cpdb.molgen.mpg.de), a web-based meta-database integrating information from around 30 different publicly available databases including WikiPathway, Reactome and KEGG (Kamburov et al., 2013), was used to identify enriched pathways in each cell culture system. The analysis was done using the ConsensusPathDB's

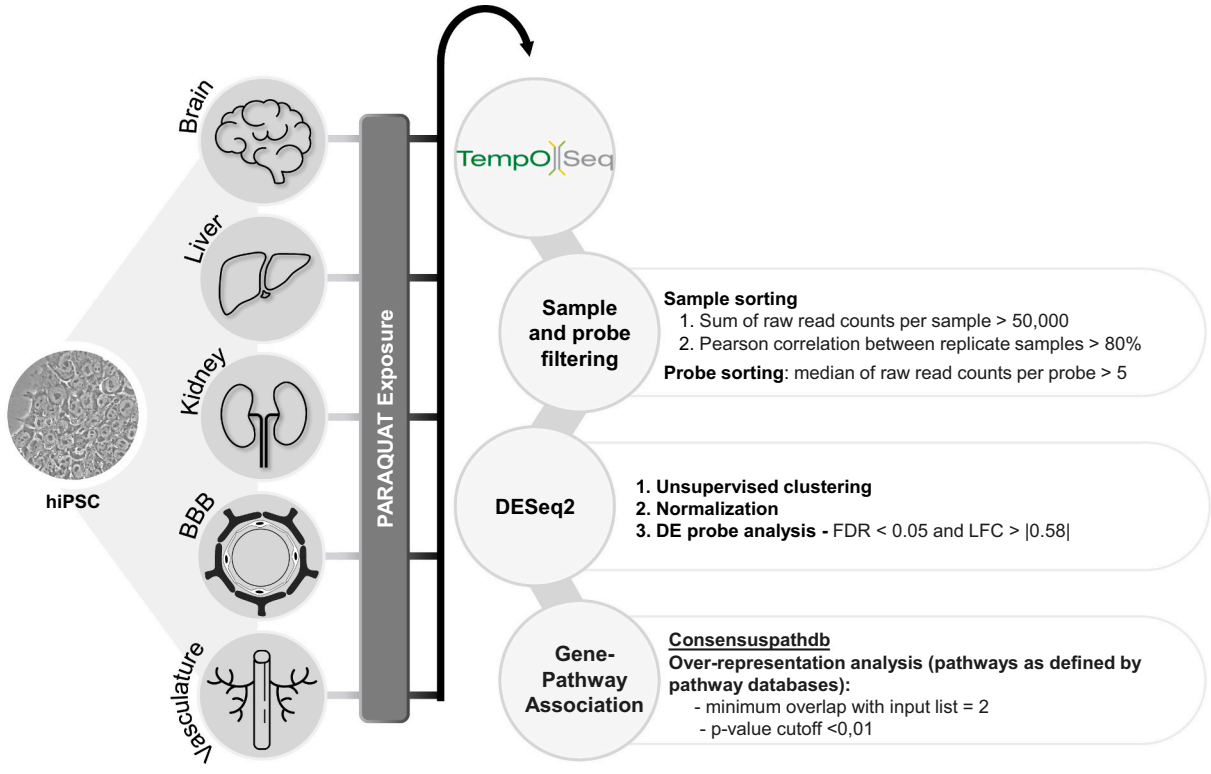

Fig. 1. *In vitro* strategy using multiple hiPSC-derived models to assess the toxicity of chemicals. Workflow used to compare the response of different hiPSC-derived cell models to PQ acute exposure based on TempOSeq data. The 7 models were differentiated from either SBAD2 or SBAD3 hiPSC lines to represent brain, liver, kidney, BBB and vasculature and exposed to different concentrations of PQ chosen on the basis of viability curves. Data from TempOSeq was analysed using R package DSeq2, after filtering and normalization of the raw data. The differentially expressed genes per model were analysed for pathway over-representation with ConsensusPathDB.

over-representation analysis (ORA) and the list of the most significantly differentially expressed genes of each system (taking all concentrations into account) as an input. HUGO gene nomenclature Committee (HGNC) symbols were employed as identifiers. ORA compares input gene list to all the genes associated to each pathway available in the databases. The default Consensus ORA settings require a minimum overlap of 2 genes between the input gene list and a given pathway associated gene list along with a *p*-value cutoff of 0.01 to define a pathway as over-represented. ORA *p*-value calculations are based on the hypergeometric distribution between the input list and existing pathway list (Kamburov et al., 2009).

2.5.4. Gene and pathway intersection analysis

To find deregulated genes and pathways shared by the different cell systems, the lists of differentially expressed genes and enriched pathways from each cell model were compared using UpSetR package (Conway et al., 2017). UpSetR package helps in both visualization and extraction of the different intersections in a matrix format by assembling different set size combinations. Mode was set to "intersect" in the function "make_comb_mat()" and the function "extract_comb()" was then used to obtain the intersections. Finally, intersection plots were created using UpSet() function in the UpSetR package (Conway et al., 2017).

3. Results

3.1. Human iPSC-derived organ-specific models exhibit different sensitivity to paraquat

In order to assess the differential sensitivity of the iPSC-derived cell models to PQ, and to choose sub-cytotoxic concentrations for subsequent experiments to elucidate early pathways of toxicity, the different iPSC-derived cell culture models were exposed to a wide range of PQ concentrations for 24 h and/or 48 h, then concentration-dependent curves for cytotoxicity were established.

The most sensitive model was found to be 2D neural cell cultures (NC), with an IC50 at 49 μM (Fig. 2 and Table 2). BS, the 3D brain cell model, was less sensitive to PQ (IC50: 200 μM after 24 h of exposure; 60 μM after 48 h). The toxicity of PQ to endothelial cells (EC) was found in the same range (IC50: 114 μM), whereas BLECs, used as a model for blood-brain barrier and later referred to as BBB, exhibited a much higher IC50 (749 μM). Among the two cell culture models representing kidney, PTL was less sensitive to PQ than PODO (IC50: 561 μM and 373 μM, respectively). Finally, the hepatocyte cell-like model (HLC) seemed to be the least sensitive model out of the seven models tested; however, the IC50 was determined only at 48 h (1093 μM, cytotoxicity data for HLC also used in Ghosh et al., submitted to Toxics) (Fig. 2 and Table 2).

The results reveal a differential response of the models to the

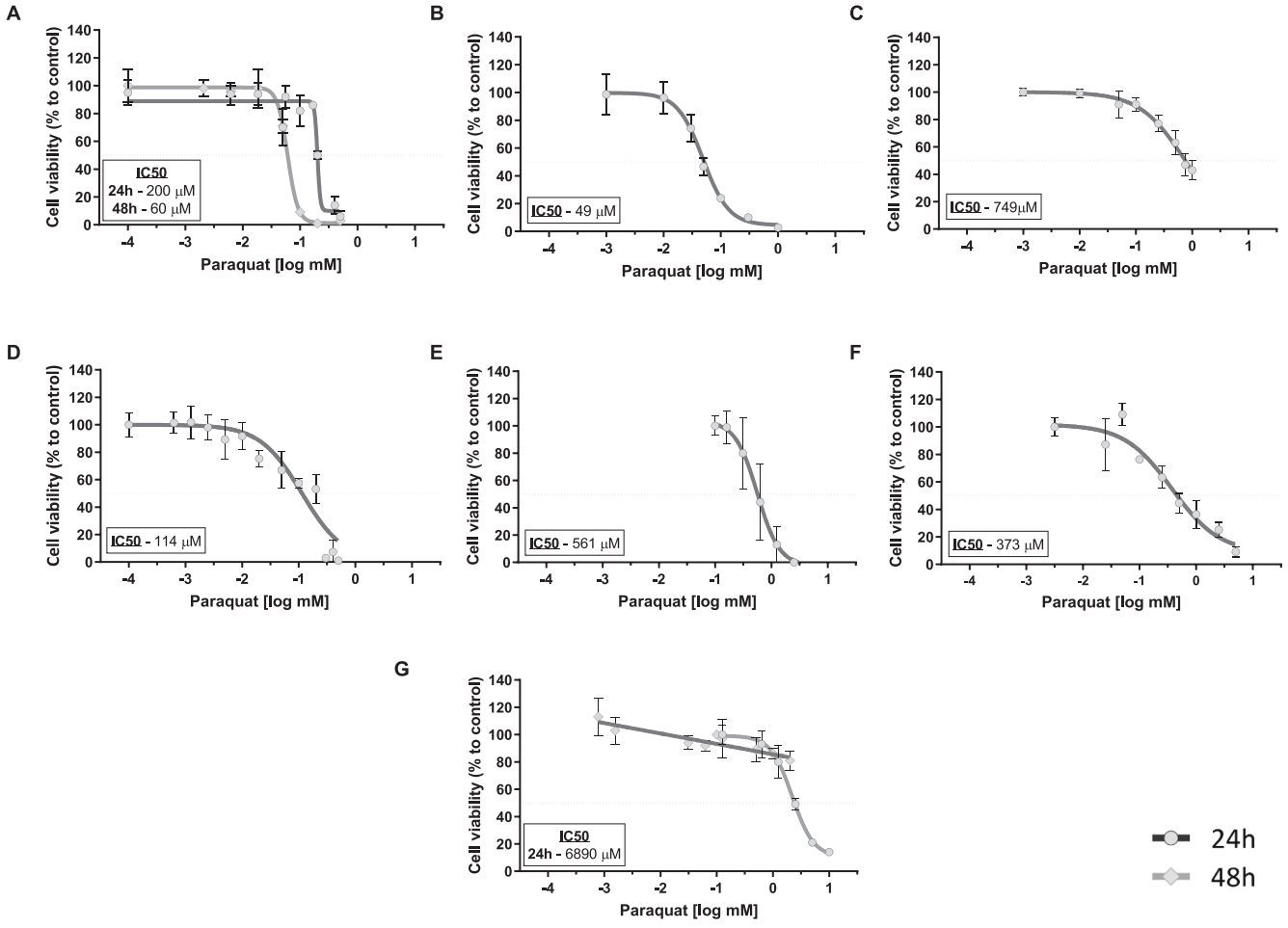

Fig. 2. Models present different sensitivity to PQ exposure. Concentration-dependent curves after 24 h and/or 48 h exposure to PQ: A) BS (0–0,5 mM), B) NC (0,001–1,5 mM), C) BLECs (0–1 mM), D) EC (0–0,5 mM), E) PTL (0–10 mM), (F) PODO (0–5 mM), G) HLC (0–10 mM; data for 48 h also used in Ghosh et al., submitted to Toxics). Results are expressed as % of control cultures a non-linear regression (log (inhibitor) *vs* response - variable slope (four parameters)) was performed in order to calculate the inhibitory concentration (IC) using GraphPad Prism®. Means ±SD of 2–9 samples obtained in 1–3 independent experiments are shown. Black line: 24 h, grey line: 48 h.

cytotoxic effects of PQ, and show that the sensitivity to PQ depend not only on the organ but also on the specific cell type considered (NC *vs* BS, modelling the brain, and PTL *vs* PODO, modelling the kidney). To identify toxicity related pathways induced by PQ, transcriptomic analysis was performed using TempO-Seq as a cost-efficient tool. Each model was exposed to at least one concentration below cytotoxicity IC10 (Table 2).

3.2. hiPSC-derived models drive sample clustering of TempO-Seq data after paraquat exposure

All human iPSC-derived models, except EC, exhibited a sum of read counts per sample above 50,000 counts, and therefore passed our first sample quality filter. The second filter, namely the Pearson correlation, led us to the elimination of one replicate of the control group from NC; two control replicates and one replicate of the 25 μM group from PTL; one replicate of treated 250 μM group from BBB and one replicate sample from the 5 μM and from the 100 μM groups from PODO. For HLC (raw data for HLC also used in Ghosh et al., submitted to Toxics) and BS, the samples from all groups showed Pearson correlation $\geq$0.80 and therefore were all kept for further analyses. For EC model, very low sums of probe read counts (5000–12,000) were found for one replicate from each treatment group and therefore these samples were also extremely poorly correlated to their corresponding replicates (Pearson correlation coefficients between 0.09 and 0.22). After removing the low correlated samples from each cell model, probes with median read counts across all samples of the model considered <5 were filtered out. This caused the removal of 1456 probes from NC, 1208 from PTL, 1445 probes from HLC, 1175 probes from BBB, 1319 probes from PODO and 1517 probes from BS. For the EC model, 64% of the probes (2097) had to be eliminated. Furthermore, although the controls of the EC model passed the 50′000 counts threshold, for undetermined reasons their read counts were much lower than in all the other models (Suppl. Fig. 1), causing a high variance potentially leading to biased normalization and distortion of the differential expression analysis. Based on these results, the data form the EC cell model were considered as unreliable, and the EC model was removed from further analyses.

After these steps of sample and probe filtering, unsupervised PCA of controls and treated samples for the 6 remaining models (Fig. 3A) showed four very distinct clusters. One cluster was formed by PODO and another cluster by HLC samples. A third cluster comprised samples from both brain models (NC and BS), whereas PTL and BBB samples were grouped together. On this PCA plot, BS was the only cell model to show clear separation between treated and control samples; however, the separation is visible when PCA is performed for each model individually, with the exception of PODO (Suppl. Fig. 2). It is remarkable that most of the variance was observed between cell models and less was due to paraquat treatment, even if the list of probes used did not comprise a lot of cell type-specific genes.

3.3. Paraquat deregulated several identical pathways in the different hiPSC-derived models

In total, we found 341 probes differentially expressed across the cell models and treatment groups upon PQ exposure. A heatmap of the 100 highest log2 FC probes (Fig. 3B), each one crossing the statistical thresholds in at least one treatment group, with values scaled for each model between the range − 1 to 1 for better relative comparison among models, clearly shows concentration-dependent effects of paraquat in the different models.

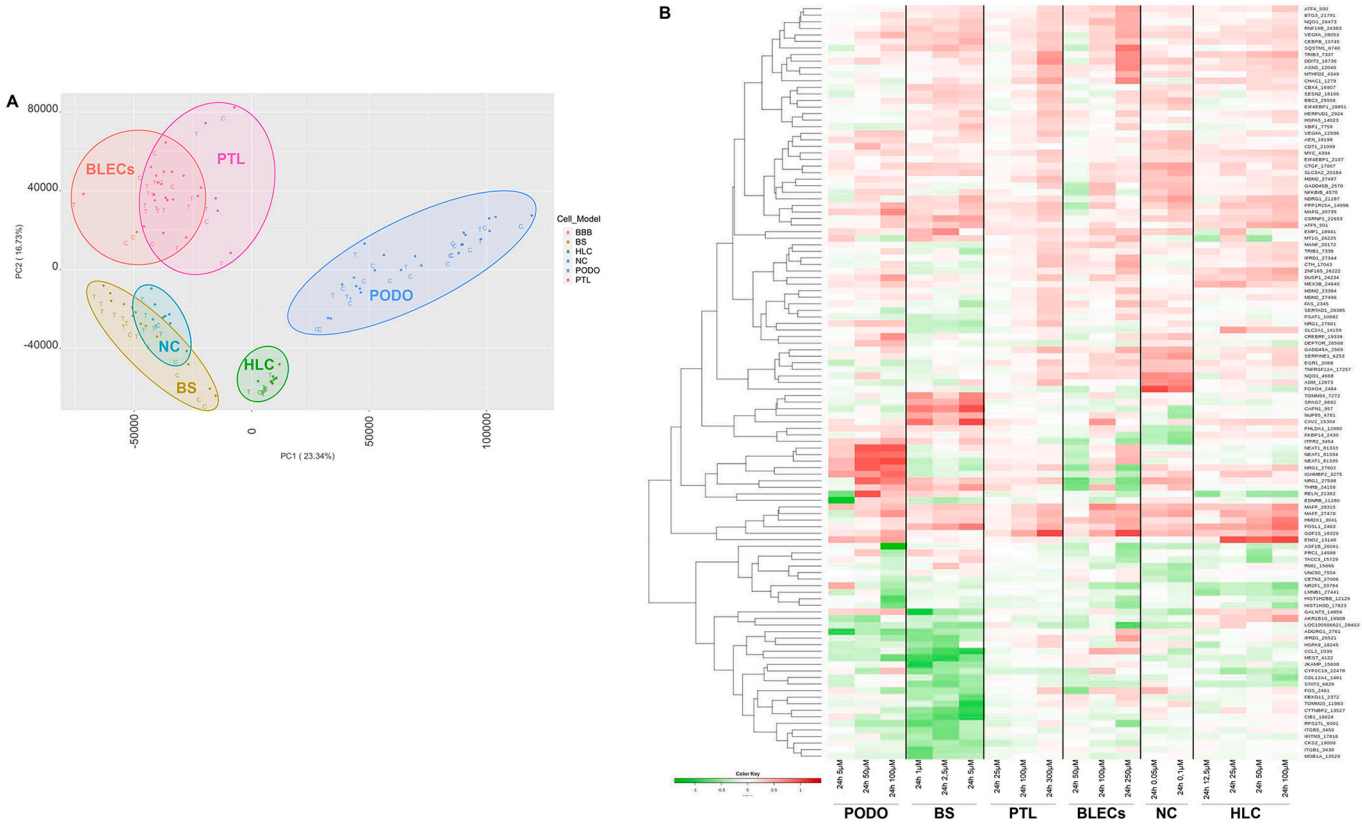

Fig. 3. Clustering of samples and the most deregulated genes after PQ exposure. A) PCA plot of all control and PQ treated samples Each dot represents a sample and each colour represents a cell model. Neuronal Cells (NC, turquoise, 2 samples), Brainsphere (BS, yellow), Podocytes (PODO, blue), Proximal tubule like cells (PTL, purple), Hepatocytes like cells (HLC, green) and Blood Brain Barrier (BLECs, pink). B) A heatmap of the 100 highest log2 FC probes (gene symbol_probe ID), each one crossing the statistical thresholds in at least one treatment group. The relative expression values scaled between −1 (green) and 1 (red).

To investigate the mechanisms of PQ toxicity shared by the different models, pathway enrichment analysis using ConsensusPathDB was performed based on the list of differentially expressed genes (DEG) derived from each model. In total, 36 pathways were identified in HLC, 110 in PODO, 136 in NC, 134 in BBB, 164 in BS and 278 pathways in PTL. The number of pathways given here includes all similar pathways described by different databases aggregated by ConsensusPathDB. Then, UpSetR package was used to find the intersections of these affected pathways in different combinations of 2, 3, 4 and 5 cell models. The pathway intersection graph (Fig. 4) shows that each cell model shared affected pathways with up to four other cell models (Fig. 4, intersections between 5 models). Furthermore, PODO and PTL that are both kidney related cell models shared 18 pathways, whereas BS and NC which are both brain-related cell models shared 17 pathways. No pathway shared by all 6 cell models was found with the criteria used in this study.

In the combinations of 5 cell models, "Oxidative stress induced gene expression via Nrf2" pathway was not found in BS (Table 3). However, read counts for Heme Oxygenase 1 (HMOX1), NAD(*P*)H Quinone Dehydrogenease (NQO1), MAF BZIP Transcription Factor F (MAFF) and G (MAFG) genes, all belonging to the oxidative stress pathway, show a concentration-dependent increase for the six models (Fig. 5), including BS. The other stress pathways found in the combination of 5 models are "Cellular responses to external stimuli" and "Cellular responses to stress" (Table 3). Among combinations of 4 cell models, many other stress pathways were identified, such as "Quercetin and Nf-kB- AP-1 Induced Cell Apoptosis", "Photodynamic therapy-induced NFE2L2 (Nrf2) survival signalling" and "Photodynamic therapy-induced unfolded protein response". Concentration-dependent increases were observed for Protein Phosphatase 1 Regulatory Subunit 15A (PPP1R15A), Activating Transcription Factor 4 (ATF4), DNA Damage Inducible Transcript 3 (DDIT3) and Asparagine Synthetase (ASNS) genes belonging to the latter pathway (UPR), even in BS, although this pathway was not identified in this model (Fig. 5). Only PODO did not show any regulation of these genes. Finally, more generic pathways such as "Cell cycle", "Cellular responses to external stimuli" and "Generic Transcription Pathway" (Table 3) were found in several combinations of four models, and "ESR-mediated signalling" pathway appeared in one of these combinations.

UpSetR package was also used to identify the genes differentially expressed in the combinations of 2, 3, 4 and 5 cell models in an unbiased way. The gene intersection graph shows that each cell model shared affected genes with up to four other cell models (Fig. 6, intersections between 5 models). No gene shared by all 6 cell models was found with the criteria used in this study. MAFF and PPP1R15A were found deregulated in 5 models (Table 4), but not in the same combination thereof, whereas Vascular Endothelial Growth Factor A (VEGFA), ATF4 and Growth Differentiation Factor 15 (GDF15) were found deregulated in 4 models. NC and BS, both CNS models, shared 6 deregulated genes (Table 4): Chromobox 4 (CBX4), Eukaryotic Translation Initiation Factor 1 (EIF1), PPP1R15A, Solute Carrier Family 3 member 2 (SLC3A2), and VEGFA, that were all upregulated in both models, as well as one downregulated gene, the tubulin alpha-1B chain (TUBA1B). Finally, PODO and PTL, models of two different kidney cell types, shared 9 upregulated genes: CD55 Molecule (CD55), Choline Kinase Alpha (CHKA), Dual Specificity Phosphatase 1 (DUSP1), Enolase 2 (ENO2), Heat Shock Protein Family A Member 1B (HSPA1B), MAFF, MAFG, PPP1R15A and VEGFA (Table 4), that were deregulated in the same direction, except for HSPA1B, downregulated in PODO but upregulated in PTL (Suppl. Fig. 3).

3.4. *Specificity of hiPSC-derived models response to Paraquat*

In addition to the cellular responses shared by the different models, we also interrogated the data for the genes that are specifically deregulated in each model. The number of deregulated probes (22–190) per model is given in Table 5. The number of down-regulated genes was very similar to the number of up-regulated genes in BS, NC and BBB models, whereas the proportion of up-regulated genes was much higher for PTL (73% of the deregulated genes), PODO (70%) and HLC (95%)

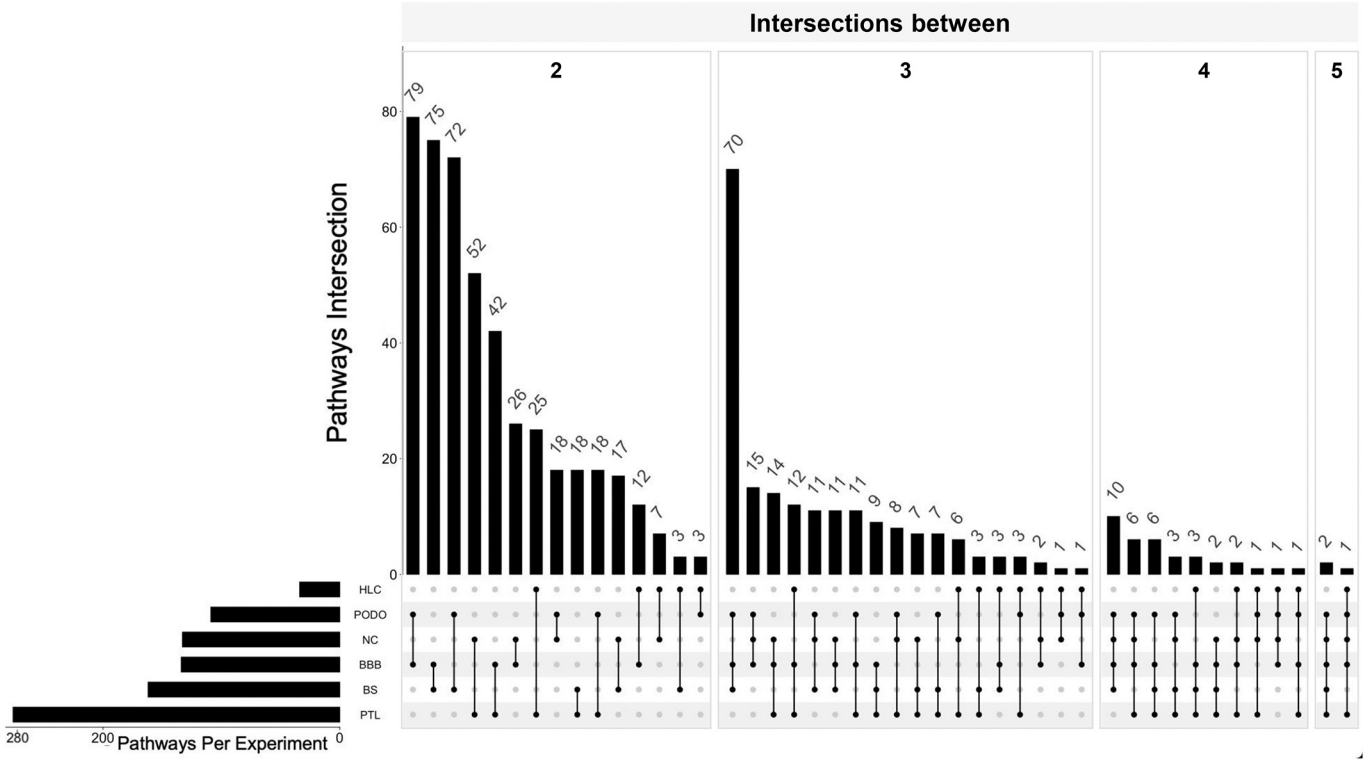

Fig. 4. All the models share perturbated pathways with at least 4 other systems. Intersection plot of the potentially affected pathways by PQ exposure shared by 2–5 models. For each model, the pathways were derived using the differentially expressed genes in the ConsensusPathDB for over-representation analysis (ORA).

Table 3
List of pathways potentially disturbed by PQ exposure in at least 4 different models.

Models	Example
NC + PODO+PTL + HLC + BBB	Oxidative stress induced gene expression *via* Nrf2
NC + BS + PODO+PTL + BBB	Cellular responses to external stimuli; Cellular responses to stress
NC + PODO+PTL + BBB	Oxidative stress induced gene expression *via* Nrf2; Cell cycle; Cellular responses to external stimuli; Cellular responses to stress; Direct p53 effectors; Generic transcription pathway
NC + BS + PODO+PTL	Cellular responses to external stimuli; Cellular responses to stress; Quercetin and Nf-kB- AP-1 induced cell apoptosis
NC + PTL + HLC + BBB	Oxidative stress induced gene expression *via* Nrf2 Photodynamic therapy-induced unfolded protein response;
NC + BS + PODO+BBB	ESR-mediated signaling; B-WICH complex positively regulates rRNA expression; Cell cycle checkpoints; Cellular responses to external stimuli; Cellular responses to stress; Epigenetic regulation of gene expression; Formation of the beta-catenin: TCF transactivating complex; Mitotic prophase; Signaling by nuclear receptors; TCF dependent signaling in response to WNT
NC + BS + PTL + BBB	Cellular responses to external stimuli; Cellular responses to stress
BS + PTL + HLC + BBB	NRF2-ARE regulation; Photodynamic therapy-induced NFE2L2 (Nrf2) survival signaling; Phytochemical activity on Nrf2 transcriptional activation
PODO+PTL + HLC + BBB	Oxidative stress induced gene expression *via* Nrf2

models (Table 5).

Among the top upregulated genes in BS (Table 5) genes involved in essential cellular functions were found, such as caveolin 2 (CAV2) and calpain 1 (CAPN1), but also genes involved in development such as SRY-BOX Transcription Factor 1 (SOX1), INSM transcriptional repressor 1 (INSM1) and Thyroid hormone receptor beta (THRB). On the other hand, the most down-regulated genes in BS were associated with cytoskeleton, such as Tubulin Alpha 1B chain (TUBA1B) and Cortactin Binding Protein 2 (CTTNBP2) and cell adhesion (Cadherin (CDH8)). In the other iPSC-derived model of brain cells, NC, the top 10 up-regulated genes included 4 genes involved in cellular stress responses, such as PPP1R15A, GDF15, Growth Arrest And DNA Damage Inducible Alpha (GADD45A) and MAFF, but also genes implicated in cell adhesion, such as Cellular Communication Network Factor 1 (CCN1 also called CYR61), Cellular Communication Network Factor 2 (CCN2 also called Connective Tissue Growth Factor (CTGF)) and Serpin Family E Member 1 (SERPINE1). In the down-regulated genes for this model, we found genes involved in mitosis (RecQ Mediated Genome Instability 1 (RMI1) and Centrin 3 (CETN3)), another one potentially mediating apoptosis during neuronal development (Pleckstrin Homology Like Domain Family A Member 1 (PHLDA1)) and an essential component of the nuclear pore complex, nucleoporin 85 (NUP85). In BBB model, most of the top ten up-regulated genes were associated with stress responses: Tribbles Pseudokinase 3 (TRIB3), DDIT3, CD55 Molecule (CD55), PPARGC1A, Sequestosome (SQSTM1), and GDF15, whereas among the top ten downregulated genes, five were histones, and one was a histone chaperone (Anti-Silencing Function 1B Histone Chaperone (ASF1B)).

For PTL, the up-regulated genes were all stress genes involved in oxidative stress and/or inflammation, except FOSL1 that is implicated in proliferation, differentiation and transformation; and among the downregulated genes are 2 genes related to detoxification (Epoxide Hydrolase 2 (EPHX2) and Aldehyde Dehydrogenase 7 Family member A1 (ALDH7A1)), as well as pyruvate dehydrogenase kinase isoenzyme 4 (PDK4), that plays a crucial role in the control of metabolic flexibility under various physiological. For the other kidney cell type, PODO, 5 of the top upregulated genes were involved in stress pathways: Matrix Metallopeptidase 2 (MMP2), Immunoglobulin Mu DNA Binding Protein 2 (IGHMBP2), CD55, MAFG and CREB3 regulatory Factor (CREBRF). Among the other upregulated genes we found Myelin Protein Zero Like 1 (MPZL1) and Ankyrin Repeat Domain 36 (ANKRD36B) involved in cell adhesion and cell membrane integrity. The downregulated genes in PODO include five histones and one histone chaperone, ASF1B, just as observed for BBB.

The model for hepatocytes, HLC, showed 6 of its top ten upregulated genes associated with oxidative stress and/or inflammation, namely the rate limiting enzyme of glutathione synthesis, Glutamate-Cysteine Ligase Modifier Subunit (GCLM), HMOX1, C-X-C Motif Chemokine Ligand 8 (CXCL8), GDF15, TRIB3 and MAFF. Besides, Ras Association Domain Family Member 1 (RASSF) involved in cell cycle and Aldo-Keto Reductase Family 1 member 1 (AKR1B10) were also upregulated. The only downregulated gene found with the criteria applied was a type of collagen (COL12A1).

Finally, basal expression of selected genes related to PQ transport, and enzymes involved in redox cycling and anti-oxidant defence were extracted from the TempO-Seq data in order to investigate their potential contribution to the sensitivity of the various models to PQ. The basal expression of Solute Carrier Family 3 Member 2 (SLC3A2) and Solute Carrier Family 7 Member 11 (SLC7A11), two amino acid transporters, was higher in BS, NC and PODO than in the other models (Fig. 7). The expression of the NAD(*P*)H-cytochrome P450 oxidoreductase (POR), involved in the redox cycling of the PQ ion, was highest in HLC than in the other models, but also robustly expressed in BS, NC and PTL. Superoxide dismutases (SOD2 and SOD3) and glutathione S-transferases (GSTA2 and GSTM3), involved in anti-oxidant defence, showed a much higher basal expression in HLC than in all the other models, even being absent from some of them, whereas SOD 1 was more expressed in BS, NC and PTL than in HLC.

4. Discussion

The development of new human-based assays for human safety assessment, highly encouraged by various authorities (EUR-Lex, 2010;

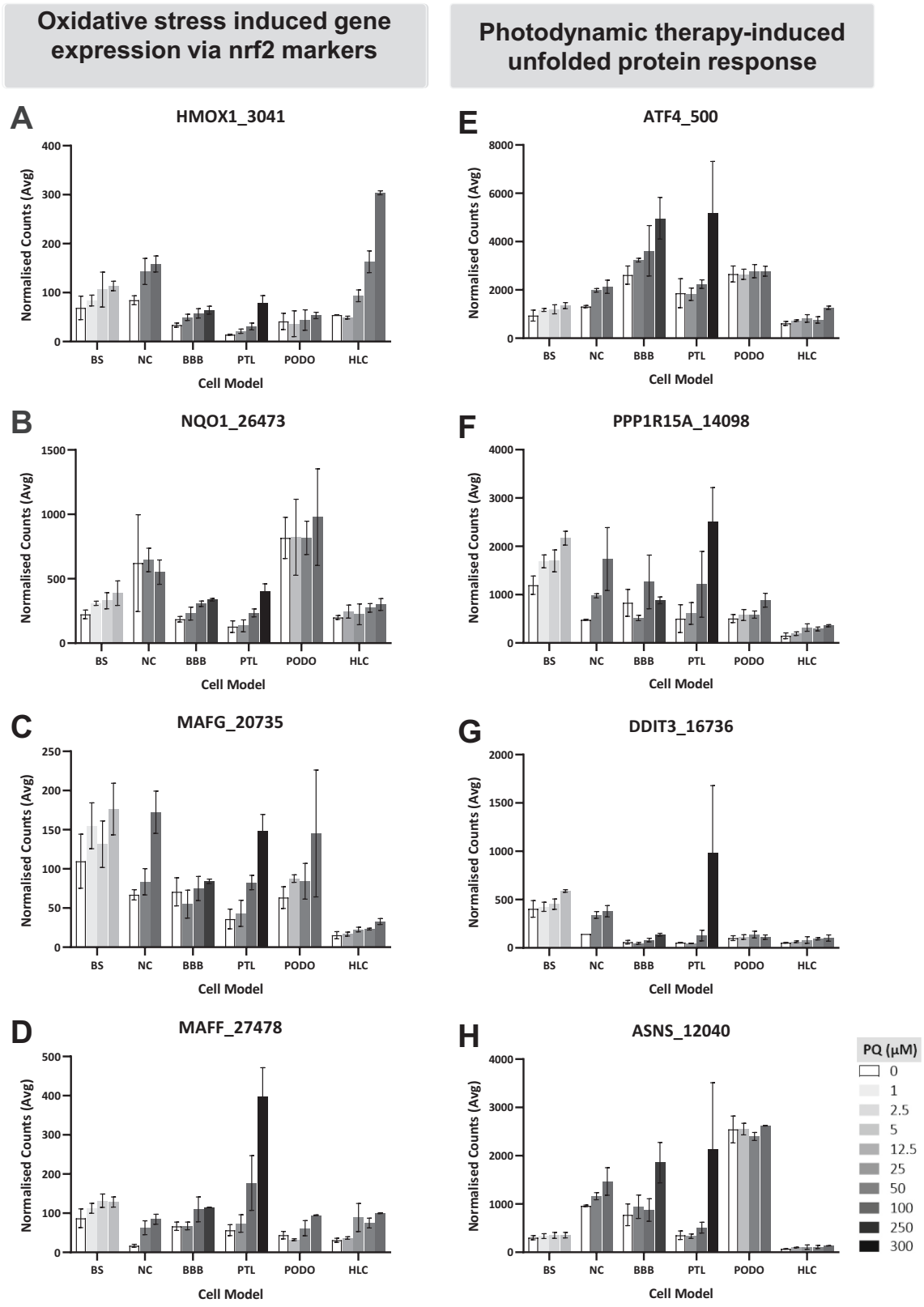

Fig. 5. PQ exposure induces upregulation of genes involved in the oxidative stress pathways Nrf2 and UPR (A-D) normalized read counts for HMOX1, NQO1, MAFG and MAFF probes (gene symbol_probe ID) involved in the "oxidative stress induced gene expression via Nrf2" pathway from BioCarta database; (*E*-H) normalized read counts for ATF4, PPP1R15A, DDIT3 and ASNS probes (gene symbol_probe ID) involved in "photodynamic therapy-induced unfolded protein response" pathway described in the Wikipathways database. Average normalized read counts ±SD are shown.

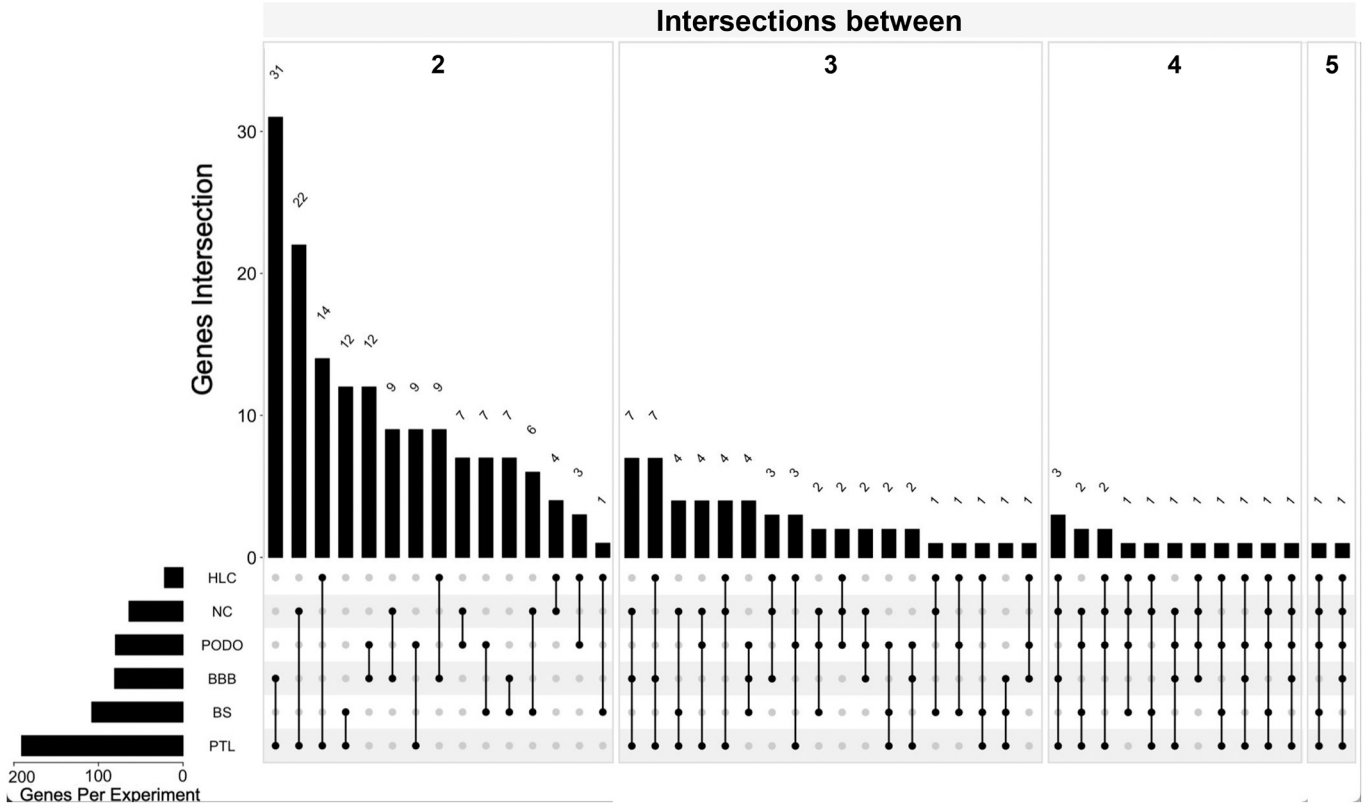

Fig. 6. All the models share differentially expressed genes with at least 4 other systems. Intersection plot of the PQ-induced DEG shared by 2–5 models using UpSetR pack. For each model, the DEG list was obtain with the DSeq2 Package.

Table 4
List of the DEGs shared by at least 4 models or by modeled organ (brain and kidney).

Organ	Intersections	Gene symbol_probe ID
	NC + PODO+PTL + HLC + BBB	MAFF_27478
	NC + BS + PODO+PTL + HLC	PPP1R15A_14098
	NC + BS + PODO+PTL	PPP1R15A_14098; VEGFA_28053
	NC + PODO+PTL + HLC	PPP1R15A_14098; MAFF_27478;
	NC + PTL + HLC + BBB	ATF4_500; GDF15_18329; MAFF_27478
Brain	NC + BS	CBX4_16907; EIF1_2074; PPP1R15A_14098; SLC3A2_20164; TUBA1B_7399; VEGFA_28053
Kidney	PODO+PTL	CD55_28297; CHKA_14315; DUSP1_24234; ENO2_13140; HSPA1B_3136; MAFF_27478; MAFG_20735; PPP1R15A_14098; VEGFA_28053

National Research Council, 2007; Oredsson et al., 2019; Sewell et al., 2017), has been made easier by the development of standardized ways to derive hiPSC from somatic cells and by the description of new methods for their differentiation into various cell types (Chandrasekaran et al., 2021; Murphy et al., 2019; Pamies et al., 2017). This raises the possibility to test for specific organ toxicity within the same genetic background to more fully assess the potential hazard of a chemical. Here we propose an *in vitro* multi-organ strategy with hiPSCs-derived models to assess the toxicity of chemicals though TempO-Seq analysis. We believe that a multi-organ approach associated with high throughput omics technology would improve the efficiency and reliability of chemical toxicity screening.

To test this approach, PQ, a herbicide widely employed with recognized toxic effects in many different organs, such as lung, kidney, central nervous system and liver (Delirrad et al., 2015; Gawarammana and Buckley, 2011; Saravu et al., 2013; Sittipunt, 2005), was used as a reference compound. The cytotoxic sensitivity to PQ we observed in this study was not the same for the different hiPSCs-derived models, with liver and kidney models being less sensitive than brain models. This is in line with a report showing that in rats, repeated, systemic low doses of PQ are much better tolerated by peripheral organs than by brain, and suggesting this to be due to easier induction of adaptive mechanisms (Kuter et al., 2010). Furthermore, this observation suggests that the application of the diverse differentiation protocols was successful. The differential sensitivity observed might be explained by the higher basal expression of amino acid transporters, such as Solute Carrier Family 3 Member 2 (SLC3A2) and Solute Carrier Family 7 Member 11 (SLC7A11), shown by TempO-Seq analysis in the most sensitive models. Indeed, amino acid transporters have been suggested to be used by PQ to enter cells (for review, see Wang et al., 2021), their stronger expression might thus potentially lead to a higher cellular uptake of PQ. The highest level of genes coding for enzymes involved in anti-oxidant defence, such as SODs and GSTs, observed in HLC, might also explain the relatively highest resistance of this model to PQ, even so NAD(*P*)H-cytochrome P450 oxidoreductase (POR), engaged in ion redox cycling of PQ was a bit more expressed in HLC. However, other genes related to transport, redox cycling and anti-oxidant defence important for PQ mode of action and cellular response were unfortunately not available in the chosen TempO-Seq panel and more experiments are needed to fully characterize the causes of the differential sensitivity to PQ observed among the

Table 5
List of the 10 most upregulated and downregulated genes after exposure to the highest concentration of PQ for each model.

Model	Downregulated			Upregulated			Total DEG
	Gene symbol_probe ID	LFC	Number (% of total)	Gene symbol_probe ID	LFC	Number (% of total)	
BS	SPC25_6704	−3.0	55 (56)	CAV2_15304	2.5	43 (44)	98
	TOMM20_11983	−2.3		CAPN1_957	2.4		
	CIB1_16624	−2.3		SPAG7_6692	1.8		
	CTTNBP2_13527	−2.2		TOMM34_7272	1.7		
	FBXO11_2372	−1.8		THRB_24158	1.4		
	TRIM2_7343	−1.4		SOX1_27894	1.4		
	TUBA1B_7399	−1.4		CSRNP1_22653	1.3		
	NDUFA4_14125	−1.4		INSM1_21254	1.2		
	CDH8_19001	−1.3		TFAP2A_7039	1.2		
	HIST1H2BG_2953	−1.3		HIF1A_2945	1.2		
NC	SGK2_10628	−6.1	30 (47)	CYR61_24505	6.3	34 (53)	64
	EDNRA_25237	−5.1		PLK1_5203	3.6		
	IFI44L_19848	−3.0		EXOSC5_27191	3.4		
	TCF4_15698	−2.6		SERPINE1_6253	2.7		
	FKBP14_2430	−2.2		CTGF_17007	2.3		
	NUP85_4781	−2.1		MAFF_27478	2.3		
	MYBL1_22509	−2.0		SLC3A2_20164	2.2		
	RMI1_15666	−2.0		GADD45A_2569	2.1		
	CETN3_27006	−1.8		GDF15_18329	1.9		
	PHLDA1_12880	−1.7		PPP1R15A_14098	1.9		
BBB	NT5DC2_4737	−2.6	43 (54)	GDF15_18329	1.9	36 (46)	79
	NCAM1_23834	−1.3		SPP1_6720	1.5		
	HMMR_3040	−1.2		SQSTM1_6740	1.5		
	HIST1H3H_2957	−1.0		PPARGC1A_12225	1.4		
	HIST1H2BG_2953	−1.0		CD55_1141	1.3		
	PSRC1_5548	−1.0		ASNS_12040	1.3		
	HIST2H2AA4_2963	−1.0		DDIT3_16736	1.2		
	HIST1H2BM_2956	−1.0		TRIB3_7337	1.2		
	HIST1H1E_14544	−1.0		CXCL2_28232	1.2		
	ASF1B_26041	−1.0		HSD17B11_3115	1.1		
PTL	CXCL14_22017	−2.2	51 (27)	GDF15_18329	6.8	139 (73)	190
	CSF3R_25969	−1.8		DDIT3_16736	4.2		
	PRR15L_5469	−1.7		NMRAL2P_81336	3.9		
	EPHX2_18456	−1.7		TRIB3_7337	3.8		
	CASP1_26966	−1.6		CHAC1_1279	3.4		
	GBP1_19263	−1.6		FOSL1_2463	3.2		
	DEPTOR_26568	−1.5		ATF3_499	3.1		
	ALDH7A1_227	−1.5		GADD45A_2569	2.9		
	CAPS_26136	−1.5		MAFF_27478	2.8		
	PDK4_28868	−1.4		IL1A_22714	2.8		
PODO	ASF1B_26041	−2.5	24 (30)	USP32P2_28186	2.2	55 (70)	79
	MYBL2_4391	−2.1		MPZL1_4249	2.1		
	HIST1H2BH_2954	−1.6		ANKRD36B_290	1.8		
	HIST1H2BB_12129	−1.4		MMP2_4213	1.8		
	HIST1H2BN_11971	−1.4		DMRTA1_14819	1.7		
	NFYB_16601	−1.3		NEAT1_81333	1.7		
	MEST_4122	−1.2		IGHMBP2_3275	1.5		
	HIST1H2BI_11969	−1.2		CD55_28297	1.5		
	IGFBP7_26667	−1.2		MAFG_20735	1.2		
	HIST2H2AA4_2963	−1.1		CREBRF_19339	1.1		
HLC	COL12A1_1461	−1.7	1 (5)	FOSL1_2463	2.7	21 (95)	22
				HMOX1_3041	2.5		
				AKR1B10_19908	1.8		
				MAFF_27478	1.7		
				GDF15_18329	1.7		
				CXCL8_14324	1.6		
				ZNF165_26222	1.6		
				TRIB3_7337	1.5		
				GCLM_25908	1.5		
				RASSF1_28369	1.5		

DEG: differentially expressed genes; LFC: log2 fold change.

various cell models. Both brain models also differ in their sensitivity to PQ. This may be explained by the cell composition and the type of cultures. The most sensitive model, NC, is a 2D model comprising neurons and a few astrocyte progenitors, whereas BS exhibit a higher astrocyte to neuron ratio, comprise oligodendrocytes and form 3D structures, possibly explaining its slightly highest resistance to paraquat.

PQ is known to produce high levels of reactive oxygen species (ROS) through mitochondrial redox cycling, and the induction of oxidative stress is one of its better described mechanisms of action in different organs (Blanco-Ayala et al., 2014; Dinis-Oliveira et al., 2008; Gawarammana and Buckley, 2011). In our study, one of the three pathways deregulated by PQ in five cell models, identified by enrichment analysis using ConsensusPathDB, was "Oxidative stress induced gene expression via Nrf2 markers". Keap1/Nrf2 activation functions mainly as an antioxidant mechanism helping cells to cope with oxidative stress and has been previously associated with PQ-induced injury (Dou et al., 2016; Kheiripour et al., 2021). Nrf2 transactivation induces the transcription of genes with upstream antioxidant response elements (ARE) to

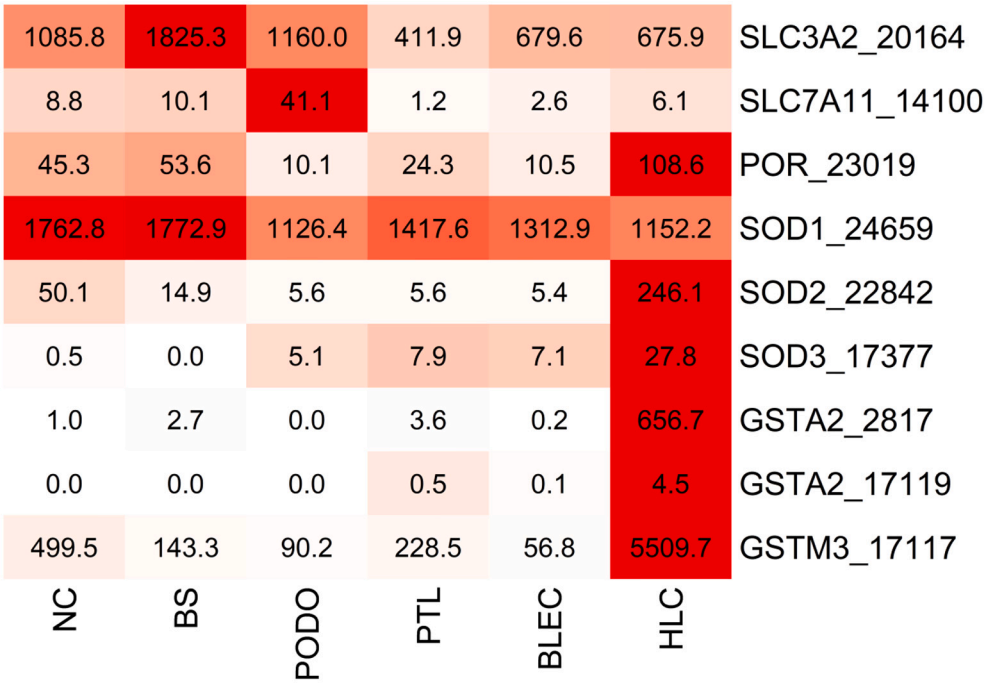

Fig. 7. Heatmap of TempO-Seq normalized read counts data for selected genes involved in PQ transport, redox cycling and anti-oxidant defence. White to red intensity represents 0 (white) to highest normalized read counts (red) of the TempO-Seq probe in the displayed data set. Annotations represent the gene symbol and Tempo-Seq probe ID. Non-normalized values are printed to allow for a quantitative comparison between genes.

counteract oxidative stress, including glutathione- reduction, −synthesis, and -recycling along with other reducing enzymes (Bugno et al., 2015; Wang et al., 2020). HMOX and NQO1 are such prototypical Nrf2 response genes (Hichor et al., 2017; Xu et al., 2017), and were induced in all the hiPSCs-derived cell systems exposed to PQ in this study. Indeed, although the thresholds were not reached to significantly activate this pathway for BS after acute exposure, we observed a concentration-dependent increase in the expression of the associated genes, and the pathway itself was impacted after 1 week of repeated exposure to PQ (Nunes et al., 2021, unpublished observation).

Endoplasmic reticulum (ER), the site of synthesis and folding of proteins, maintains a strict quality control targeting incorrectly folded proteins for proteasomal degradation (Smith et al., 2011). Upon accumulation of protein-folding alterations occurring during ER stress, cells activate a series of complementary adaptive mechanisms, the unfolded protein response (UPR), primarily serving to return normal ER function, and failure to adapt to ER stress may result in apoptosis triggered by UPR (Hetz, 2012; Lin and LaVail, 2010). Perturbations in ER calcium, high ROS production, depletion of oxidised glutathione and proteotoxicity all have the potential to activate the UPR. Indeed, disturbance of ER and UPR have been described in human lung epithelial cells after PQ exposure (Chinta et al., 2008; Omura et al., 2013). Furthermore, recently UPR was reported after PQ treatment in primary cultures of human CD34+ derived dendritic cells, but not in macrophages (Fransen and Leonard, 2021). In the present study, the UPR pathway was highlighted in four out of the six models. As for the oxidative stress pathway, a repeated exposure to PQ was necessary to detect the UPR using ConsensusPathBD in BrainSpheres (Nunes et al., 2021, unpublished observation), although a clear concentration-dependent increase was observed in the expression of several genes involved in this pathway, such as ATF4, PPP1R15A and DDIT3, already after 24 h of exposure. The second model, for which ConsensusPathDB did not highlight UPR, the podocyte model (PODO), showed only a slight modification of PPP1R15A, suggesting no or only very weak activation of UPR-PERK branch, contrary to the observation made in the other kidney cell type, PTL. Further studies are needed to determine whether PQ activates UPR through the induction of ER stress, as described in lung epithelial cells, or directly through the induction of ROS, since an interaction between UPR and oxidative stress has been described (Kupsco and Schlenk, 2015), involving the phosphorylated form of eIF2α, ATF4, CHOP (transcription factor C/EBP homologous protein, also called DDIT3) and PPP1R15A (Harding et al., 2009; Hetz, 2012; Pavitt and Ron, 2012; Tabara et al., 2018). Altogether, our results show that even though we used a minimum overlap of two genes between the input gene list and a given pathway associated gene list to define a pathway as overrepresented, our strategy using several hiPSC-derived models, with various cell type or organ specificities, allowed to detect the main mechanisms of action of PQ.

Another pathway revealed after PQ exposure in four cell culture systems, including both brain models (NC and BS), BLECs and HLC, was “ESR-mediated signaling”. This is interesting given that estrogenic dysfunction has recently been identified to be involved in toxicity induced by PQ on rat primary hippocampal neurons *in vitro* (Moyano et al., 2020a, 2020b) and that estradiol has been shown to protect a neuronal line from PQ toxicity (Gélinas et al., 2004). It is therefore remarkable to note that our strategy not only retrieved the main, known mechanisms of action of PQ, but also a recently proposed one that clearly deserves further studies.

Most of the top ten upregulated genes per model were involved in stress responses, in particular oxidative stress and inflammation for four hiPSC-derived models out of the six tested. The two brain models, NC and BS, however behaved differently, exhibiting genes involved in development, such as OX1 and INSM1 that promote generation and expansion of neuronal progenitor cells, and the thyroid receptor that is also important in the development and maintenance of brain structures. The lower proportion of genes involved in stress responses among the top upregulated genes in brain models suggest that brain cells have the weakest self-defence capacity against toxins or can less easily induce their adaptative mechanisms than peripheral organs (Kuter et al., 2010). These results show that although stress pathways shared by most of the models have been identified, each model seemed to also react in a specific way to paraquat. This is remarkable since in this study we used a

restricted number of probes, that were not specifically designed for cell type-specific discrimination.

Finally, VEGFA was induced by PQ in four of the models. VEGFA, a prototypical HIF1 alpha gene, primarily induced as a response to hypoxia, is mainly known for its activities related to angiogenesis, vascular permeability and vascular survival (Ferrara, 2004). There is a growing body of evidence, however, that VEGFA fulfils additional less 'traditional' functions in multiple organs during development, as well as homeostatic functions in fully developed organs (for review, see (Licht and Keshet, 2013)). Our results showing the upregulation of VEGFA shared by both brain models and both kidney models are perfectly in line with the current knowledge on the importance of VEGFA for these two organs. VEGFA, mainly expressed in astrocytes and neurons is upregulated in all brain cell types upon severe hypoxia (Jin et al., 2000). It is also expressed in glomerular podocytes, where it is critical for the establishment and maintenance of glomerular filtration (Eremina et al., 2003), and ample evidence supports important roles for this growth factor in the maintenance of tubulointerstitial integrity and the response to acute kidney injury (Doi et al., 2010; Schrijvers et al., 2004). The upregulation of VEGFA in brain and kidney models after exposure to PQ, again shows that the hiPSCs-derived models used in this study are reproducing the organ patho-physiology, and furthermore suggests this growth factor as marker of chemical injury.

Some limitations of the study should be stated. The cell models utilised here although from the same donors were cultured, differentiated and treated separately. Our systems and the majority of *in vitro* models in general represent a reductionist approach and does not fully reflect the physiology of a whole organism due to the lack of connections and communications between them through blood flow, endocrine and nervous systems. This could possibly be better recapitulated in the future by using organ-on-a-chip models and/or by the application of *in silico* modelling. Furthermore, the iPSCs-derived models used in this study, beside their great advantages, come also with some limitations. For example, although the BS model is multicellular and highly complex it does not (at this point in development) possess microglia, precluding the development of the full neuroinflammatory cascade. The HLC are not completely mature hepatocytes and lack cooperation with Kupfer cells, and the kidney model PODO lacks fenestrated endothelial cells and glomerular basement membrane to form a full glomerular model. These limitations can be overcome in the near future by co-culturing cells with their missing partners. Finally, in order to overcome the multiple differences linked to cell culture conditions that could impact the true comparisons of the effects of PQ in the different models, the distribution kinetics of PQ has to be established for each model, to correlate the observed toxic effects to the effective concentrations reaching the cells and not to the nominal concentrations used. This will allow a better comparison of the effects of chemicals on the various models.

5. Conclusions

Our strategy, taking advantage of the iPSC technology, allowed to determine the known and less known mechanisms of PQ toxicity with TempO-Seq analysis, using a cost-effective panel of probes specific for toxicity testing. The main advantages of this strategy are to assess chemical toxicity on cell types from multiple organs in parallel, exclusively in human cells, eliminating interspecies bias and allowing a better evaluation of the differential sensitivity of the models representing the diverse organs. To apply this approach to the general assessment of chemical toxicity, the strategy presented herein could be further improved by adding hiPSC-derived models for other organs, such as the heart and the lungs, and by standardization of procedures to reach a higher level of harmonization between the different laboratories. Furthermore, organ-specific toxicity testing could be reached by adding organ-specific genes to our set of TempO-Seq probes.

Given the present results showing the differential sensitivity of the various human models to PQ, we believe this strategy will contribute to the further improvement of chemical risk assessment for human health, providing the above cited improvements combined with the evaluation of the distribution kinetics of the chemicals, as a key step for the *in vitro* to *in vivo* extrapolation (IVIVE) (Punt et al., 2020), absolutely required for regulatory decision-making.

Supplementary data to this article can be found online at https://doi.org/10.1016/j.tiv.2022.105333.

Declaration of Competing Interest

The authors declare no competing interests.

Acknowledgements

The work was funded by the European Union's Horizon 2020 Research and Innovation Programme MarieSklodowska-Curie Action-Innovative Training Network project in3, under grant agreement no. 721975 (fellowships to Carolina Nunes, Pranika Singh, Zahra Mazidi, Cormac Murphy, Aurore Bourguignon, Sara Wellens, Vidya Chandrasekaran and Sreya Ghosh).

References

Blanco-Ayala, T., Andérica-Romero, A.C., Pedraza-Chaverri, J., 2014. New insights into antioxidant strategies against paraquat toxicity. Free Radic. Res. 48, 623–640. https://doi.org/10.3109/10715762.2014.899694.

Boon, R., Kumar, M., Tricot, T., Elia, I., Ordovas, L., Jacobs, F., One, J., De Smedt, J., Eelen, G., Bird, M., Roelandt, P., Doglioni, G., Vriens, K., Rossi, M., Vazquez, M.A., Vanwelden, T., Chesnais, F., El Taghdouini, A., Najimi, M., Sokal, E., Cassiman, D., Snoeys, J., Monshouwer, M., Hu, W.S., Lange, C., Carmeliet, P., Fendt, S.M., Verfaillie, C.M., 2020. Amino acid levels determine metabolism and CYP450 function of hepatocytes and hepatoma cell lines. Nat. Commun. 11, 1–16. https://doi.org/10.1038/s41467-020-15058-6.

Bugno, M., Daniel, M., Chepelev, N.L., Willmore, W.G., 2015. Changing gears in Nrf1 research, from mechanisms of regulation to its role in disease and prevention. Biochim. Biophys. Acta - Gene Regul. Mech. 1849, 1260–1276. https://doi.org/10.1016/j.bbagrm.2015.08.001.

Chambers, S.M., Fasano, C.A., Papapetrou, E.P., Tomishima, M., Sadelain, M., Studer, L., Author, N.B., 2009. Highly efficient neural conversion of human ES and iPS cells by dual inhibition of SMAD signaling HHS Public Access Author manuscript. Nat. Biotechnol. 27, 275–280. https://doi.org/10.1038/nbt.1529.

Chandrasekaran, A., Avci, H.X., Ochalek, A., Rösingh, L.N., Molnár, K., László, L., Bellák, T., Téglási, A., Pesti, K., Mike, A., Phanthong, P., Bíró, O., Hall, V., Kitiyanant, N., Krause, K.H., Kobolák, J., Dinnyés, A., 2017. Comparison of 2D and 3D neural induction methods for the generation of neural progenitor cells from human induced pluripotent stem cells. Stem Cell Res. 25, 139–151. https://doi.org/10.1016/j.scr.2017.10.010.

Chandrasekaran, V., Carta, G., Pereira, C., Gupta, R., Murphy, C., Feifel, E., Kern, G., Lechner, J., Cavallo, A.L., Gupta, S., Caiment, F., Kleinjans, J.C.S., Gstraunthaler, G., 2021. Generation and characterization of iPSC – derived renal proximal tubule – like cells with extended stability. Sci. Rep. 1–17 https://doi.org/10.1038/s41598-021-89550-4.

Chinta, S.J., Rane, A., Poksay, K.S., Bredesen, D.E., Andersen, J.K., Rao, R.V., 2008. Coupling endoplasmic reticulum stress to the cell death program in dopaminergic cells: effect of paraquat. Neuro Mol. Med. 10, 333–342. https://doi.org/10.1007/s12017-008-8047-9.

Cicchetti, F., Drouin-Ouellet, J., Gross, R.E., 2009. Environmental toxins and Parkinson's disease: what have we learned from pesticide-induced animal models? Trends Pharmacol. Sci. 30, 475–483. https://doi.org/10.1016/j.tips.2009.06.005.

Conway, J.R., Lex, A., Gehlenborg, N., 2017. UpSetR: an R package for the visualization of intersecting sets and their properties. Bioinformatics 33, 2938–2940. https://doi.org/10.1093/bioinformatics/btx364.

Delirrad, M., Majidi, M., Boushehri, B., 2015. Clinical features and prognosis of paraquat poisoning: a review of 41 cases. J. Clin. Exp. Med 8 (5), 8122–8128.

Dinis-Oliveira, R.J., Duarte, J.A., Sánchez-Navarro, A., Remião, F., Bastos, M.L., Carvalho, F., 2008. Paraquat poisonings: mechanisms of lung toxicity, clinical features, and treatment. Crit. Rev. Toxicol. 38, 13–71. https://doi.org/10.1080/10408440701669959.

Doi, K., Noiri, E., Fujita, T., 2010. Role of vascular endothelial growth factor in kidney disease. Curr. Vasc. Pharmacol. 8, 122–128. https://doi.org/10.2174/157016110790226606.

Dou, T., Yan, M., Wang, X., Lu, W., Zhao, L., Lou, D., Wu, C., Chang, X., Zhou, Z., 2016. Nrf2/ARE pathway involved in oxidative stress induced by paraquat in human neural progenitor cells. Oxidative Med. Cell. Longev. 2016 https://doi.org/10.1155/2016/8923860.

EPA, 2019. Administrator Memo Prioritizing Efforts to Reduce Animal Testing, September 10, 2019. United States Environ. Prot. Agency.

Eremina, V., Sood, M., Haigh, J., Nagy, A., Lajoie, G., Ferrara, N., Gerber, H.P., Kikkawa, Y., Miner, J.H., Quaggin, S.E., 2003. Glomerular-specific alterations of

VEGF-A expression lead to distinct congenital and acquired renal diseases. J. Clin. Invest. 111, 707–716. https://doi.org/10.1172/JCI17423.
EUR-Lex, 2010. Directive 2010/63/EU of the European parliament and of the Council of 22 September 2010 on the protection of animals used for scientific purposes. Off. J. Eur. Union 1–61.
Ferrara, N., 2004. Vascular endothelial growth factor: basic science and clinical progress. Endocr. Rev. https://doi.org/10.1210/er.2003-0027.
Fransen, L.F.H., Leonard, M.O., 2021. CD34+ derived macrophage and dendritic cells display differential responses to paraquat. Toxicol. in Vitro 75, 105198. https://doi.org/10.1016/j.tiv.2021.105198.
Gao, L., Yuan, H., Xu, E., Liu, J., 2020. Toxicology of paraquat and pharmacology of the protective effect of 5-hydroxy-1-methylhydantoin on lung injury caused by paraquat based on metabolomics. Sci. Rep. 10, 4–8. https://doi.org/10.1038/s41598-020-58599-y.
Gawarammana, I.B., Buckley, N.A., 2011. Medical management of paraquat ingestion. Br. J. Clin. Pharmacol. 72, 745–757. https://doi.org/10.1111/j.1365-2125.2011.04026.x.
Gélinas, S., Bureau, G., Valastro, B., Massicotte, G., Cicchetti, F., Chiasson, K., Gagne, B., Blanchet, J., Martinoli, M.G., 2004. Alpha and beta estradiol protect neuronal but not native PC12 cells from paraquat-induced oxidative stress. Neurotox. Res. 6, 141–148. https://doi.org/10.1007/BF03033216.
Gholami, S., Mazidi, Z., Pahlavan, S., Moslem, F., Hosseini, M., Taei, A., Hesaraki, M., Barekat, M., Aghdami, N., Baharvand, H., 2021. A novel insight into endothelial and cardiac cells phenotype in systemic sclerosis using patient-specific induced pluripotent stem cell. Cell J. 23 https://doi.org/10.22074/cellj.2021.7244.This.
Harding, H.P., Zhang, Y., Scheuner, D., Chen, J.J., Kaufman, R.J., Ron, D., 2009. Ppp1r15 gene knockout reveals an essential role for translation initiation factor 2 alpha (eIF2α) dephosphorylation in mammalian development. Proc. Natl. Acad. Sci. U. S. A. 106, 1832–1837. https://doi.org/10.1073/pnas.0809632106.
Herrmann, K., Pistollato, F., Stephens, M.L., 2019. Food for thought … beyond the 3Rs: expanding the use of human-relevant replacement methods in biomedical research. ALTEX 36, 343–352. https://doi.org/10.14573/altex.1907031.
Hetz, C., 2012. The unfolded protein response: controlling cell fate decisions under ER stress and beyond. Nat. Rev. Mol. Cell Biol. 13, 89–102. https://doi.org/10.1038/nrm3270.
Hichor, M., Sampathkumar, N.K., Montanaro, J., Borderie, D., Petit, P.X., Gorgievski, V., Tzavara, E.T., Eid, A.A., Charbonnier, F., Grenier, J., Massaad, C., 2017. Paraquat induces peripheral myelin disruption and locomotor defects: crosstalk with LXR and Wnt pathways. Antioxid. Redox Signal. 27, 168–183. https://doi.org/10.1089/ars.2016.6711.
Jin, K.L., Mao, X.O., Nagayama, T., Goldsmith, P.C., Greenberg, D.A., 2000. Induction of vascular endothelial growth factor and hypoxia-inducible factor-1α by global ischemia in rat brain. Neuroscience 99, 577–585. https://doi.org/10.1016/S0306-4522(00)00207-4.
Kamburov, A., Wierling, C., Lehrach, H., Herwig, R., 2009. ConsensusPathDB - a database for integrating human functional interaction networks. Nucleic Acids Res. 37, 623–628. https://doi.org/10.1093/nar/gkn698.
Kamburov, A., Stelzl, U., Lehrach, H., Herwig, R., 2013. The ConsensusPathDB interaction database: 2013 update. Nucleic Acids Res. 41, 793–800. https://doi.org/10.1093/nar/gks1055.
Kheiripour, N., Plarak, A., Heshmati, A., Asl, S.S., Mehri, F., Ebadollahi-Natanzi, A., Ranjbar, A., Hosseini, A., 2021. Evaluation of the hepatoprotective effects of curcumin and nanocurcumin against paraquat-induced liver injury in rats: modulation of oxidative stress and Nrf2 pathway. J. Biochem. Mol. Toxicol. 1–9 https://doi.org/10.1002/jbt.22739.
Kupsco, A., Schlenk, D., 2015. Oxidative Stress, Unfolded Protein Response, and Apoptosis in Developmental Toxicity, International Review of Cell and Molecular Biology. Elsevier Ltd. https://doi.org/10.1016/bs.ircmb.2015.02.002
Kuter, K., Nowak, P., Gołembiowska, K., Ossowska, K., 2010. Increased reactive oxygen species production in the brain after repeated low-dose pesticide paraquat exposure in rats. A comparison with peripheral tissues. Neurochem. Res. 35, 1121–1130. https://doi.org/10.1007/s11064-010-0163-x.
Li, H., Durbin, R., 2009. Fast and accurate short read alignment with burrows-wheeler transform. Bioinformatics 25, 1754–1760. https://doi.org/10.1093/bioinformatics/btp324.
Licht, T., Keshet, E., 2013. Delineating multiple functions of VEGF-A in the adult brain. Cell. Mol. Life Sci. https://doi.org/10.1007/s00018-013-1280-x.
Limonciel, A., Ates, G., Carta, G., Wilmes, A., Watzele, M., Shepard, P.J., VanSteenhouse, H.C., Seligmann, B., Yeakley, J.M., van de Water, B., Vinken, M., Jennings, P., 2018. Comparison of base-line and chemical-induced transcriptomic responses in HepaRG and RPTEC/TERT1 cells using TempO-Seq. Arch. Toxicol. 92, 2517–2531. https://doi.org/10.1007/s00204-018-2256-2.
Lin, J.H., LaVail, M.M., 2010. Misfolded Proteins and Retinal Dystrophies, in: Advances in Experimental Medicine and Biology. Springer, New York, NY, pp. 115–121. https://doi.org/10.1007/978-1-4419-1399-9_14.
Liu, S., Yin, N., Faiola, F., 2017. Prospects and Frontiers of stem cell toxicology. Stem Cells Dev. 26, 1528–1539. https://doi.org/10.1089/scd.2017.0150.
Lo Giudice, M., Mihalik, B., Turi, Z., Dinnyés, A., Kobolák, J., 2019. Calcilytic NPS 2143 reduces amyloid secretion and increases sAβPPα release from PSEN1 mutant iPSC-derived neurons. J. Alzheimers Dis. 72, 885–899. https://doi.org/10.3233/JAD-190602.
Love, M.I., Huber, W., Anders, S., 2014. Moderated estimation of fold change and dispersion for RNA-seq data with DESeq2. Genome Biol. 15, 550. https://doi.org/10.1186/s13059-014-0550-8.
Mav, D., Shah, R.R., Howard, B.E., Auerbach, S.S., Bushel, P.R., Collins, J.B., Gerhold, D. L., Judson, R.S., Karmaus, A.L., Maull, E.A., Mendrick, D.L., Merrick, B.A., Sipes, N. S., Svoboda, D., Paules, R.S., 2018. A hybrid gene selection approach to create the S1500+ targeted gene sets for use in high-throughput transcriptomics. PLoS One 13, e0191105. https://doi.org/10.1371/JOURNAL.PONE.0191105.
Morrison, M., Klein, C., Clemann, N., Collier, D.A., Hardy, J., Heiβerer, B., Cader, M.Z., Graf, M., Kaye, J., 2015. StemBANCC: governing access to material and data in a large stem cell research consortium. Stem Cell Rev. Rep. 11, 681–687. https://doi.org/10.1007/s12015-015-9599-3.
Moyano, P., Sanjuan, J., García, J.M., Anadon, M.J., Lobo, M., Pelayo, A., García, J., Frejo, M.T., del Pino, J., 2020a. Primary hippocampal estrogenic dysfunction induces synaptic proteins alteration and neuronal cell death after single and repeated paraquat exposure. Food Chem. Toxicol. 136, 110961 https://doi.org/10.1016/j.fct.2019.110961.
Moyano, P., Sanjuan, J., García, J.M., Anadon, M.J., Naval, M.V., Sola, E., García, J., Frejo, M.T., Pino, J. del, 2020b. Dysregulation of prostaglandine E2 and BDNF signaling mediated by estrogenic dysfunction induces primary hippocampal neuronal cell death after single and repeated paraquat treatment. Food Chem. Toxicol. 144 https://doi.org/10.1016/j.fct.2020.111611.
Murphy, C., Feifel, E., Jennings, P., Gstraunthaler, G., Wilmes, A., 2019. A protocol for One-step differentiation of human induced pluripotent stem cells into mature podocytes. In: Mandenius, C.-F., Ross, J.A. (Eds.), Cell-Based Assays Using iPSCs for Drug Development and Testing. Springer, New York, New York, NY, pp. 93–99. https://doi.org/10.1007/978-1-4939-9477-9_8.
National Research Council, 2007. Toxicity Testing in the 21st Century: A Vision and a Strategy [WWW Document]. Natl. Acad. Press, Washington, DC. URL. https://books.google.ch/books?hl=pt-PT&lr=&id=3AWfAwAAQBAJ&oi=fnd&pg=PT21&dq=Toxicity+Testing+in+the+21st+Century:+A+Vision+and+a+Strategy&ots=UwnqSFwazc&sig=KCxUqgElnoh_RuE2YHTzTTuNRMU&redir_esc=y#v=onepage&q=ToxicityTestinginthe21stCentury%3AAVis (accessed 4.30.21).
Nunes, C., Zurich, M.-G., 2020. Neurotoxicology and Disease Modelling. Springer, Cham, pp. 229–246. https://doi.org/10.1007/978-3-030-43939-2_12.
Ochalek, A., Mihalik, B., Avci, H.X., Chandrasekaran, A., Téglási, A., Bock, I., Giudice, M. Lo, Táncos, Z., Molnár, K., László, L., Nielsen, J.E., Holst, B., Freude, K., Hyttel, P., Kobolák, J., Dinnyés, A., 2017. Neurons derived from sporadic Alzheimer's disease iPSCs reveal elevated TAU hyperphosphorylation, increased amyloid levels, and GSK3B activation. Alzheimers Res. Ther. 9, 1–19. https://doi.org/10.1186/s13195-017-0317-z.
Omura, T., Asari, M., Yamamoto, J., Oka, K., Hoshina, C., Maseda, C., Awaya, T., Tasaki, Y., Shiono, H., Yonezawa, A., Masuda, S., Matsubara, K., Shimizu, K., 2013. Sodium tauroursodeoxycholate prevents paraquat-induced cell death by suppressing endoplasmic reticulum stress responses in human lung epithelial A549 cells. Biochem. Biophys. Res. Commun. 432, 689–694. https://doi.org/10.1016/j.bbrc.2013.01.131.
Oredsson, S., Coecke, S., van der Valk, J., Vinken, M., 2019. What is understood by "animal-free research"? Toxicol. in Vitro 57, 143–144. https://doi.org/10.1016/j.tiv.2019.03.001.
Pamies, D., Barreras, P., Block, K., Makri, G., Kumar, A., Wiersma, D., Smirnova, L., Zhang, C., Bressler, J., Christian, K.M., Harris, G., Ming, G.L., Berlinicke, C.J., Kyro, K., Song, H., Pardo, C.A., Hartung, T., Hogberg, H.T., 2017. A human brain microphysiological system derived from induced pluripotent stem cells to study neurological diseases and toxicity. ALTEX 34, 362–376. https://doi.org/10.14573/altex.1609122.
Pavitt, G.D., Ron, D., 2012. New insights into translational regulation in the endoplasmic reticulum unfolded protein response. Cold Spring Harb. Perspect. Biol. 4, 1–13. https://doi.org/10.1101/cshperspect.a012278.
Punt, A., Bouwmeester, H., Blaauboer, B.J., Coecke, S., Hakkert, B., Hendriks, D.F.G., Jennings, P., Kramer, N.I., Neuhoff, S., Masereeuw, R., Paini, A., Peijnenburg, A.A.C. M., Rooseboom, M., Shuler, M.L., Sorrell, I., Spee, B., Strikwold, M., Van der Meer, A. D., Van der Zande, M., Vinken, M., Yang, H., Bos, P.M.J., Heringa, M.B., 2020. New approach methodologies (NAMs) for human-relevant biokinetics predictions. Meeting the paradigm shift in toxicology towards an animal-free chemical risk assessment. ALTEX 37, 607–622. https://doi.org/10.14573/altex.2003242.
Rauch, C., Feifel, E., Kern, G., Murphy, C., Meier, F., Parson, W., Beilmann, M., Jennings, P., Gstraunthaler, G., Wilmes, A., 2018. Differentiation of human iPSCs into functional podocytes. PLoS One 13. https://doi.org/10.1371/journal.pone.0203869.
Saravu, K., Sekhar, S., Pai, A., Barkur, A.S., Rajesh, V., Earla, J.R., 2013. Paraquat – a deadly poison: report of a case and review. Indian J. Crit. Care Med. 17, 182–184. https://doi.org/10.4103/0972-5229.117074.
Schrijvers, B.F., Flyvbjerg, A., De Vriese, A.S., 2004. The role of vascular endothelial growth factor (VEGF) in renal pathophysiology. Kidney Int. 65, 2003–2017. https://doi.org/10.1111/j.1523-1755.2004.00621.x.
Sevin, E., Dehouck, L., Versele, R., Culot, M., Gosselet, F., 2019. A miniaturized pump out method for characterizing molecule interaction with ABC transporters. Int. J. Mol. Sci. 20 https://doi.org/10.3390/ijms20225529.
Sewell, F., Aggarwal, M., Bachler, G., Broadmeadow, A., Gellatly, N., Moore, E., Robinson, S., Rooseboom, M., Stevens, A., Terry, C., Burden, N., 2017. The current status of exposure-driven approaches for chemical safety assessment: a cross-sector perspective. Toxicology 389, 109–117. https://doi.org/10.1016/j.tox.2017.07.018.
Singh, P., Chandrasekaran, V., Hardy, B., Wilmes, A., Jennings, P., Exner, T.E., 2021. Temporal transcriptomic alterations of cadmium exposed human iPSC-derived renal proximal tubule-like cells. Toxicol. in Vitro 73.
Sittipunt, C., 2005. Paraquat Poisoning.
Smith, M.H., Ploegh, H.L., Weissman, J.S., 2011. Road to ruin: targeting proteins for degradation in the endoplasmic reticulum. Science (80-.). https://doi.org/10.1126/science.1209235.

Steimberg, N., Bertero, A., Chiono, V., Dell'Era, P., Di Angelantonio, S., Hartung, T., Perego, S., Raimondi, M., Xinaris, C., Caloni, F., de Angelis, I., Alloisio, S., Baderna, D., 2020. iPS, organoids and 3d models as advanced tools for in vitro toxicology. ALTEX 37, 136–140. https://doi.org/10.14573/altex.1911071.

Tabara, K., Iwata, Y., Koizumi, N., 2018. The unfolded protein response. Methods Mol. Biol. 1691, 223–230. https://doi.org/10.1007/978-1-4939-7389-7_17.

Takahashi, K., Tanabe, K., Ohnuki, M., Narita, M., Ichisaka, T., Tomoda, K., 2007. Induction of Pluripotent Stem Cells from Adult Human Fibroblasts by Defined Factors, pp. 861–872. https://doi.org/10.1016/j.cell.2007.11.019.

Wang, X., Zhang, Y., Wan, X., Guo, C., Cui, J., Sun, J., Li, L., 2020. Responsive expression of MafF to β -amyloid-induced oxidative stress. Dis. Markers 2020. https://doi.org/10.1155/2020/8861358.

Wang, X., Wang, X., Zhu, Y., Chen, X., 2021. ADME/T-based strategies for paraquat detoxification: transporters and enzymes. Environ. Pollut. 291, 118137 https://doi.org/10.1016/j.envpol.2021.118137.

Wellens, S., Dehouck, L., Chandrasekaran, V., Singh, P., Loiola, R.A., Sevin, E., Exner, T., Jennings, P., Gosselet, F., Culot, M., 2021. Evaluation of a human iPSC-derived BBB model for repeated dose toxicity testing with cyclosporine A as model compound. Toxicol. in Vitro 73, 105112. https://doi.org/10.1016/j.tiv.2021.105112.

Xu, W., Li, F., Xu, Z., Sun, B., Cao, J., Liu, Y., 2017. Tert-butylhydroquinone protects PC12 cells against ferrous sulfate-induced oxidative and inflammatory injury via the Nrf2/ARE pathway. Chem. Biol. Interact. 273, 28–36. https://doi.org/10.1016/j.cbi.2017.05.021.

Zhou, T., Benda, C., Duzinger, S., Huang, Y., Li, X., Li, Y., Guo, X., Cao, G., Chen, S., Hao, L., Chan, Y.C., Ng, K.M., Ho, J.C., Wieser, M., Wu, J., Redl, H., Tse, H.F., Grillari, J., Grillari-Voglauer, R., Pei, D., Esteban, M.A., 2011. Generation of induced pluripotent stem cells from urine. J. Am. Soc. Nephrol. 22, 1221–1228. https://doi.org/10.1681/ASN.2011010106.